# A Genetic Screen for Suppressors and Enhancers of the Drosophila Cdk1-Cyclin B Identifies Maternal Factors That Regulate Microtubule and Microfilament Stability

**Jun-Yuan Ji,* Marjan Haghnia,† Cory Trusty,* Lawrence S. B. Goldstein† and Gerold Schubiger*,[1]**

**Department of Zoology, University of Washington, Seattle, Washington 98195-1800 and †Department of Cellular and Molecular Medicine, School of Medicine, Howard Hughes Medical Institute, University of California, San Diego, California 92093-0683*

Manuscript received December 19, 2001
Accepted for publication July 8, 2002

ABSTRACT

Coordination between cell-cycle progression and cytoskeletal dynamics is important for faithful transmission of genetic information. In early Drosophila embryos, increasing maternal cyclin B leads to higher Cdk1-CycB activity, shorter microtubules, and slower nuclear movement during cycles 5–7 and delays in nuclear migration to the cortex at cycle 10. Later during cycle 14 interphase of *six cycB* embryos, we observed patches of mitotic nuclei, chromosome bridges, abnormal nuclear distribution, and small and large nuclei. These phenotypes indicate disrupted coordination between the cell-cycle machinery and cytoskeletal function. Using these sensitized phenotypes, we performed a dosage-sensitive genetic screen to identify maternal proteins involved in this process. We identified 10 suppressors classified into three groups: (1) gene products regulating Cdk1 activities, *cdk1* and *cyclin A*; (2) gene products interacting with both microtubules and microfilaments, *Actin-related protein 87C*; and (3) gene products interacting with microfilaments, *chickadee*, *diaphanous*, *Cdc42*, *quail*, *spaghetti-squash*, *zipper*, and *scrambled*. Interestingly, most of the suppressors that rescue the astral microtubule phenotype also reduce Cdk1-CycB activities and are microfilament-related genes. This suggests that the major mechanism of suppression relies on the interactions among Cdk1-CycB, microtubule, and microfilament networks. Our results indicate that the balance among these different components is vital for normal early cell cycles and for embryonic development. Our observations also indicate that microtubules and cortical microfilaments antagonize each other during the preblastoderm stage.

A typical somatic cell cycle contains M phase (mitosis) and S phase (DNA synthesis) separated by two gap phases, G1 and G2. In contrast, the early embryonic cycles of insects, marine invertebrates, and amphibians consist of only M and S phases without gap phases (Murray and Hunt 1993). In Xenopus, translation of Cyclin B (CycB) is both necessary and sufficient for progression of the early embryonic cycles (Murray and Kirschner 1989; Nurse 1990). Cdk1-CycB destabilizes microtubules in Xenopus egg extracts, indicating that it regulates microtubule dynamics (Verde *et al.* 1990). In cultured mammalian cells, Cdk1-CycB has been shown to regulate microfilament dynamics by phosphorylating caldesmon, a necessary event for disassembly of microfilaments during M phase (Yamashiro *et al.* 2001). Using early Drosophila embryos, we investigated how coordination between Cdk1-CycB and the two major dynamic cytoskeletal networks is accomplished.

As in Xenopus, fluctuation of Cdk1-CycB activity controls the progression of the first 14 embryonic cycles in Drosophila (Edgar *et al.* 1994; Hartley *et al.* 1996). After fertilization, the first four cycles occur deep in the center and slightly toward the anterior of the embryo. During each prophase and metaphase of cycles 4–7, the nuclei migrate along the anterior-posterior axis in a process known as axial expansion, which depends on both microtubules and microfilaments (Zalokar and Erk 1976; Baker *et al.* 1993). Later during telophase and interphase of cycles 7–10, nuclei undergo microtubule-dependent cortical migration (Foe and Alberts 1983; Baker *et al.* 1993). The following four syncytial blastoderm cycles become increasingly slower, with cycle 14 interphase lasting at least 1 hr.

Comparing the early cycles of Drosophila (cycles 1–10) and Xenopus (cycles 2–12), there are two important differences with respect to cell-cycle regulation. First, CycB protein levels oscillate in Xenopus, but such global oscillations are detected only after cycle 6 in Drosophila (Edgar *et al.* 1994). Second, Cdk1 is periodically inactivated by transient Tyr15 phosphorylation in Xenopus (Kim *et al.* 1999) but not in Drosophila (Edgar *et al.* 1994). It is still possible that inhibitory phosphorylation on Cdk1 might occur locally during the preblastoderm cycles. However, progression of the preblastoderm cycles is normal in embryos from mutant mothers lacking the kinases responsible for the inhibitory phosphate, such as *Dwee1*, *mei-41*, or *grapes* (Sibon *et al.* 1997, 1999; Price *et al.* 2000). How do these early embryonic cell

[1]*Corresponding author:* Department of Zoology, University of Washington, Seattle, WA 98195-1800. E-mail: gerold@u.washington.edu

cycles progress without inactivating Cdk1? One possibility is that cell-cycle control is executed locally by CycB. In support of this idea, injection of nondegradable CycB protein into preblastoderm embryos leads to local cell-cycle arrest in the area of injection (Su *et al.* 1998). In addition, in preblastoderm cycles CycB disappears from microtubules during the metaphase-anaphase transition (Stiffler *et al.* 1999), supporting local rather than global oscillation of CycB (Edgar *et al.* 1994; Su *et al.* 1998). Local degradation of CycB on spindle microtubules is also observed later during cycles 10–13 (Huang and Raff 1999). Thus, local CycB levels may define Cdk1-CycB activity and drive nuclear division during the preblastoderm stage.

An important gap in our understanding is how the cell-cycle machinery, particularly Cdk1-CycB, interacts with the cytoskeletal network. To address this question, we performed a genetic screen on the basis of responses to dosage changes of maternal CycB levels induced during cycles 1–14. Embryos with higher Cdk1-CycB activity have longer metaphase and shorter microtubules before cycle 10 (Stiffler *et al.* 1999). In embryos with 6 copies of maternal *cycB*, we frequently observed abnormalities such as patches of mitotic nuclei, chromosome bridges, and uneven nuclear distribution at cycle 14 interphase. Similar but more severe phenotypes were observed in embryos with as many as 10 doses of maternal *cycB*, which arrested as early as cycle 3 (Stiffler *et al.* 1999). Thus, a screen to enhance or suppress these phenotypes was performed to find genes that link the cytoskeletal machinery to the cell-cycle machinery.

## MATERIALS AND METHODS

**Stocks and crosses:** Flies were raised at 25° on cornmeal molasses medium. Control data were from wild-type "Sevelen" flies. Animals with eight copies of *cycB* (*P*-element-mediated germ-line insertion of a 10-kb genomic *cycB* fragment on chromosomes II and III) were kindly provided by C. Lehner (Jacobs *et al.* 1998). Deficiency lines (see Appendix at http://www.genetics.org/supplemental/) covering ~70% of the Drosophila genome were received from the Bloomington and Umea stock centers. Descriptions of these lines can be found at FlyBase (http://flybase.bio.indiana.edu/; FlyBase Consortium 1999). We received *Apc2* from A. Bejsovec. T. Grigliatti provided *cdk1* alleles $cdk1^{216P}$, $cdk1^{B47}$, $cdk1^{D57}$, and $cdk1^{E1\text{-}24}$ (Clegg *et al.* 1993; Stern *et al.* 1993). L. Cooley sent us *chickadee* (*chic*) and *quail* (*qua*) mutants. $chic^{0135}$ ($chic^{10}$), $chic^{4205}$ ($chic^{13}$), $chic^{7772}$ ($chic^{14}$), $chic^{8893}$ ($chic^{15}$), and $chic^{7886}$ are hypomorphic alleles (Cooley *et al.* 1992; Castrillon *et al.* 1993) and $chic^{0281}$ is an amorphic allele (Verheyen and Cooley 1994). All three *qua* alleles, $qua^{WP165}$, $qua^{HM14}$ ($qua^{9}$), and $qua^{PX42}$ ($qua^{10}$) were generated by EMS mutagenesis (Steward and Nüsslein-Volhard 1986; Schüpbach and Wieschaus 1991). C. Lehner gave us a *cyclin A* (*cycA*) hypomorphic allele $cycA^{neo114}$ and an amorphic allele $cycA^{C8LR1}$. S. Wasserman provided us with a *diaphanous* (*dia*) null allele $dia^{2}$ and two hypomorphic alleles $dia^{1}$ and $dia^{9}$ (Castrillon and Wasserman 1994). S. Campbell sent us $Dwee^{DS1}$ and $Dwee^{ES1}$ and D. St. Johnston gave us $par\text{-}1^{w3}$. α- and β-*spectrin* and $\beta_{(Heavy)}$-*spectrin* mutants were obtained from G. Thomas. D. Kiehart sent a hypomorphic *spaghetti-squash* (*sqh*) allele $sqh^{1}$ and a null allele $sqh^{2}$ (Karess *et al.* 1991; Edwards and Kiehart 1996). *Merlin* mutant $Mer^{3}$ and two *Cdc42* mutants, a hypomorphic allele $Cdc42^{2}$ and a null allele $Cdc42^{4}$, were received from R. Fehon (Genova *et al.* 2000). W. Sullivan provided the $scrambled^{1}$ (*sced*) allele and the $grapes^{1}$ (*grp*) allele (Sullivan *et al.* 1993). All other mutant stocks were obtained from the Bloomington stock center.

Females with deficiencies or mutations in a background with two *cycB* copies (designated as "*mutation/+*") or with six *cycB* copies (*e.g.*, *w/+; mutation/2P[$w^{+}$ cycB]; 2P[$w^{+}$ cycB]/+*, designated as "*mutation/six cycB*") were generated by the following crosses: First chromosome *mutant/Balancer* virgins were crossed to wild-type or *w; 2P[$w^{+}$ cycB]/ CyO; 2P[$w^{+}$ cycB]* males; second and third chromosome *mutant/Balancer* males were crossed to wild-type or *w; 2P[$w^{+}$ cycB]/ CyO; 2P[$w^{+}$ cycB]* virgins. Duplications covering the deficiencies were outcrossed. To avoid possible paternal effects, female offspring were crossed to wild-type males.

**Phenotypic analyses:** Embryo collections were done as described by Stiffler *et al.* (1999). Hatching rates of all lines were calculated 26 hr after egg deposition. Hatching rates were used only as a preliminary screen to select putative suppressors or putative enhancers (see results), which were further analyzed at cycle 14.

Cycle 14 phenotypes were analyzed from fixed embryos (1-hr collection after precollections, aged 2.5 hr from midpoint). Embryos were dechorionated as described (Theurkauf 1992), fixed for 10 min in 6% formaldehyde [in PBS-0.1% Triton X-100 (PBS-Tx)] under heptane, and devitellinized with cold methanol. Embryos were stained in 4′, 6-diamidino-2-phenyindole (Sigma, St. Louis) solution (1 μg/ml in PBS) for 9–10 min, rinsed, and mounted in glycerol:10× PBS (9:1). We analyzed the embryos with a Nikon Microphot-FX fluorescence microscope using a 20× objective. Cycle 14 embryos were scored by counting number of nuclei in the midsagittal optical section (Newman and Schubiger 1980). Representative images of cycle 14 phenotypes (Figure 2) were generated from embryos fixed in 20% formaldehyde and stained with rabbit anti-phospho-histone H3 polyclonal antibody (Upstate Biotechnology, Lake Placid, NY; 1:1000 in PBS-Tx) to identify mitoses and with a mouse antihistone monoclonal antibody (Chemicon International, Temecula, CA; 1:500 in PBS-Tx) to visualize nuclei. To compare the percentage of normal embryos between different genotypes (Tables 1 and 2), we performed Pearson's chi-square test and calculated a 95% confidence interval for all the percentage data using StatXact 4.0 (Cytel Software).

Cycle 10 analysis was based on both time-lapse videos (see below) and fixed embryos. After precollections, 30-min collections were made and embryos were aged for 90 min from the midpoint and fixed in 20% formaldehyde. The embryos were immunostained with antihistone antibody (Stiffler *et al.* 1999), and nuclear distribution at cycle 10 was analyzed with a fluorescence microscope. We counted the total number of nuclei to determine cycle 10. We found ~10–15% of overaged embryos.

**Metaphase astral microtubule analyses:** Embryos were fixed in fresh 20% formaldehyde (in PBS with 0.1% NP-40) and stained with antibodies against tubulin and histone as described by Stiffler *et al.* (1999). Images were collected from a Bio-Rad (Richmond, CA) MRC-600 confocal microscope using a Plan Apochromatic 60× oil immersion lens (Figures 4 and 6). Three-micrometer Z-sections were made through the nuclei-containing midsagittal sections of cycles 5–7 embryos. To determine the percentage of metaphase spindles with asters in each embryo, all the images were analyzed using NIH Image (from http://rsb.info.nih.gov/nih-image/) without prior processing. We used StatXact 4.0 to perform the Wilcoxon-Mann-Whitney test on these data (Table 3).

**Microfilament staining:** Wild-type embryos staged between cycles 7 and 9 were dechorionated in bleach and then fixed for 15–16 min in a fixative cocktail containing 30% methanol-free paraformaldehyde (from 40% electron-microscopy grade paraformaldehyde solution; Electron Microscopy Sciences, Fort Washington, PA) and 5% methanol diluted in PBS-Tx (modified from von Dassow and Schubiger 1994; Foe *et al.* 2000). The embryos were rinsed with PBS and hand-devitellinized with tungsten needles. Devitellinized embryos were rinsed with PBS-Tx and incubated with BODIPY 558/568 phalloidin (Molecular Probes, Eugene, OR; 10 units/ml) and rhodamine-conjugated antihistone antibody (1:500) in PBS-Tx for 5 hr at room temperature. BODIPY-phalloidin was used because it gives better microfilament staining than other phallotoxin derivatives for Drosophila embryos (von Dassow and Schubiger 1994). Embryos were washed three times with PBS-Tx (15 min each) and three times with PBS (10 min each), dehydrated in 30, 50, 70, 90, and 95% PBS, and then dehydrated three times in 100% isopropanol. The dehydration process was finished within 15 min and embryos were then mounted in Murray mounting medium.

**Cytochalasin D treatment:** We permeabilized wild-type embryos so that cytochalasin D (cytD) can enter the embryos. For this we modified the protocols described by Limbourg and Zalokar (1973), Mitchison and Sedat (1983), and Theurkauf (1992). Embryos between cycles 6 and 8 were dechorionated with bleach and then put into a test tube containing 500 μl octane and 500 μl Ringer's solution with or without 50 μg/ml cytD. The embryos in this two-phase mixture were incubated for 10 min with gentle shaking. The Ringer solution (with or without cytD) was then replaced with fixatives and fixed embryos were stained for microtubules or microfilaments by using the methods described in the previous two sections. The control embryos display normal cytoskeletal networks and cell-cycle progression using this method of treatment and fixation.

**Cdk1-CycB kinase assay:** The kinase assay was performed according to Stiffler *et al.* (1999) with the difference that we used six embryos between cycles 5 and 7 for each sample and used a Phosphoimager (Bio-Rad) to quantify levels of radiolabeled histone H1. For each assay (*e.g.*, Figure 4D), we used two independent samples of wild-type and two samples of *six cycB* embryos as controls and two independent samples of embryos for each genotype (experimental embryos). The mean value of quantified radioactivity of the *six cycB* embryos was set as 100%, and the kinase activity of experimental embryos was compared to *six cycB* embryos and normalized as a percentage of the *six cycB* embryos of the same assay (Table 3). For each genotype, we repeated the assay with 4–12 independent samples (Table 3). We conducted two types of loading controls. First, we took 500 μl of supernatant of each sample after immunoprecipitation with anti-CycB serum (Rb271) and used Western blots to test actin levels within the supernatant of different samples. These data are not shown since this control confirms only the same input of different samples. The second control used two independent samples of wild-type embryos with each kinase assay. The second control is better because all samples went through all steps of the kinase assay with the experimental embryos. Therefore, these control data are presented in Table 3. Statistical analyses were performed by using S-PLUS (the one-sample *t*-test) and StatXact 4.0 (the Wilcoxon signed-rank test for one-sample data).

**Time-lapse video analysis:** Embryos were collected, hand-dechorionated with forceps, mounted onto a double-stick tape-covered slide, and then covered with halocarbon oil. Axial expansion analysis was determined by time-lapse video analysis (Stiffler *et al.* 1999). We defined cell-cycle phases and the number and duration of axial expansion cycles by tracking the movements of migrating energids (Baker *et al.* 1993). We used the Mann-Whitney rank test to compare cell-cycle duration and number among different genotypes (Zar 1999).

## RESULTS

**Sensitized phenotypes of *six cycB* embryos and design of a dosage-sensitive genetic screen:** In Drosophila, the zygotic nucleus undergoes nine divisions within the central portion of the embryo. The entire population of somatic nuclei reaches the periphery during a 2-min interval at cycle 10 (Figures 1 and 5A). In embryos from mothers with six copies of *cycB* (*six cycB* embryos), nuclei reach the periphery later and nonsynchronously (Figures 1 and 5B); it takes more than one cycle for a uniform distribution of nuclei at the cortex to form. In wild-type embryos during cycle 14 interphase, the nuclei are evenly spaced at the cortex and they stay in interphase for at least 60 min (Figures 1 and 2A). This normal cycle 14 phenotype was observed in 97% of wild-type embryos. However, 26% of *six cycB* embryos have patches of mitotic nuclei during cycle 14 interphase and areas of lower nuclear density (Figures 1 and 2B). Occasionally, we observed chromosomal bridges and macro- and micronuclei. Nevertheless, the *six cycB* embryos have only a slightly reduced larval hatching rate (92% compared to 96% in control embryos).

Using the cycle 14 phenotype of *six cycB* embryos described above, we performed a dosage-sensitive genetic screen to identify genes that when reduced in dosage would dominantly enhance or suppress the *six cycB* phenotypes. The use of deficiency lines enables the survey of a large portion of the genome and targets a few specific suppressor or enhancer regions for further analyses (for examples, see Kennison and Tamkun 1988; Nicholls and Gelbart 1998; Li *et al.* 2000; Lee *et al.* 2001).

For an initial screen, the hatching rate of *six cycB* embryos was compared to that of *six cycB* embryos with heterozygous deficiencies or mutations of specific genes (*Df/six cycB* or *mutation/six cycB*). To eliminate mutations that nonspecifically decreased hatching rates, we tested deficiencies or mutations in a wild-type background (*Df/+* or *mutation/+*; see Appendix at http://www.genetics.org/supplemental/ for specific data). Putative enhancers were identified if the hatching rate of *Df/six cycB* (or *mutation/cycB*) was at least 45% lower than that of *Df/+* (or *mutation/+*) embryos. *Df/six cycB* (or *mutation/six cycB*) embryos with high hatching rates (>90%) were selected as putative suppressors.

All putative enhancers and suppressors identified on the basis of the hatching rate criterion were then analyzed for the percentage of normal cycle 14 embryos. Compared to the cycle 14 phenotype of *six cycB* embryos, enhancer *Df/six cycB* embryos had a more severe cycle 14 phenotype (Figure 2C) and a significantly lower percentage of normal cycle 14 embryos (<20%, Table 1).

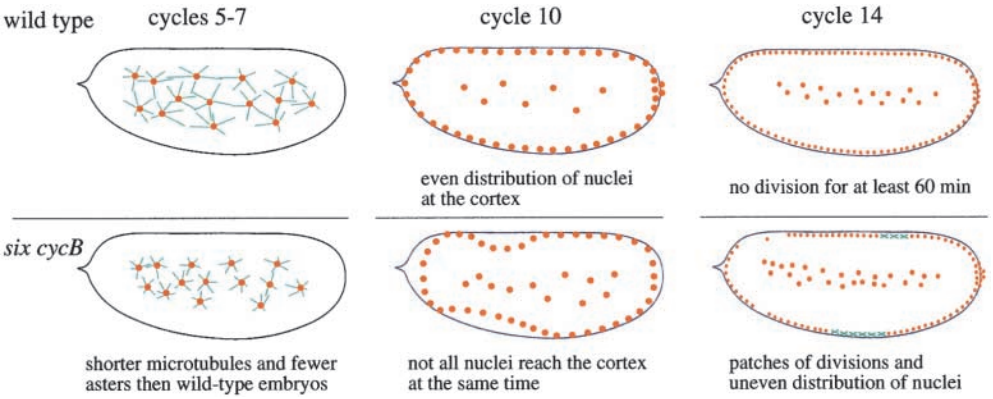


FIGURE 1.—Schematic phenotypes of wild-type and *six cycB* embryos at cycles 5–7, 10, and 14. Note that compared to wild-type embryos, there are shorter microtubules and fewer astral microtubules in *six cycB* embryos at cycles 5–7, there is an uneven distribution and penetration of nuclei into the cortex at cycle 10, and there are patches of mitosis (green) and uneven nuclear distribution during cycle 14 interphase.

In contrast, suppressor *Df/six cycB* embryos have a normalized cycle 14 phenotype (Figure 2D) and a significantly higher percentage of normal cycle 14 embryos (Table 1). The cycle 14 phenotype of all putative enhancer and suppressor lines was also analyzed using a point system. We scored the following abnormalities: patches of local division (Figure 2B), patches of lower nuclear densities (Figure 2, B and C), chromosomal bridges (Figure 2C), and macro- or micronuclei (Figure 2C) or preblastoderm arrest. Total scores were divided by the number of embryos analyzed as an average score for each genotype. Since point scores and percentages of the normal cycle 14 embryos (no division during cycle 14 interphase) led to the same conclusions, we have presented only the percentage data of the normal cycle 14 embryos in Tables 1 and 2. To investigate the mechanisms of enhancement and suppression of the *six cycB* phenotypes, we further analyzed some deficiencies and mutant genes during cycles 5–7 and at cycle 10 (see below).

**Survey of deficiencies for enhancers and suppressors of the *six cycB* phenotypes:** Hatching rates of 159 deficiency lines, covering ~70% of the Drosophila euchromatic genome, were tested in both wild-type and *six cycB* backgrounds (Figure 3; see Appendix at http://www.genetics.org/supplemental/).

**Enhancers:** The analysis of hatching rates led us to identify 18 putative enhancers (see Appendix at http://www.genetics.org/supplemental/; putative enhancers and suppressors are in boldface type), which were then analyzed for their cycle 14 phenotype (Figure 1). Compared to those of the *six cycB* embryos, 13 of these 18 putative enhancer lines had a significantly more severe cycle 14 phenotype (20% or fewer normal embryos; Figure 2C, Table 1). These 13 lines were selected as enhancers.

To rule out possible effects due to genetic background and also to narrow down the region of interaction, we retested the enhancer regions, using different and partial overlapping deficiencies. One enhancer line, *Df(2L)GdphA*, at cytogenetic map region 25–26 of the salivary gland polytene chromosome (referred to as "cytogenetic map"), was excluded (Figure 3, marked with X) because other deficiency lines covering this region did not enhance the *six cycB* phenotypes (see Figure 3 and Appendix at http://www.genetics.org/supplemental/ for details).

The remaining 12 enhancer lines define six cytogenetic map regions. In region 38A1; 40B1, we found four enhancing deficiencies: *Df(2L)TW84*, *Df(2L)TW161*, *Df(2L)TW1*, and *Df(2L)DS6* (Figure 3, Table 1). They overlap in region 38E2; 39C2–3. Three enhancing deficiencies, *Df(2R)Pcl7B*, *Df(2R)PC4*, and *Df(2R)Pcl11B*, map to region 54E8–F1; 55F1–2 and overlap between 55A1 and 55B9–C1. In region 70–71, we found two enhancing deficiencies, *Df(3L)fzGF3b* and *Df(3L)fzM21*, deleting regions 70C2; 70D5 and 70D2; 71E4–5, respectively, overlapping at 70D2; 70D5. However, *Df(3L)fz-GS1a*, which covers this overlapping region at 70D2; 70E4–5, suppressed the *six cycB* cycle 14 phenotype (Table 1). Therefore, there may be two enhancers flanking the suppressor region 70D2; 70E4–5. Finally, *Df(1)N19* covers region 17A1; 18A2, *Df(2R)AA21* covers 56F9–11; 57D12, and *Df(3L)Ar14-8* covers region 61C4; 62A8.

**Suppressors:** A total of 26 *Df/six cycB* lines have high hatching rates (>90%), and they were identified as putative suppressors (boldface type in the Appendix at http://www.genetics.org/supplemental/). In 12 of these lines, we observed a significantly higher percentage (>81%) of normal cycle 14 embryos and a less severe cycle 14 phenotype compared to *six cycB* embryos (Figure 2D, Table 1). These 12 lines covering nine different chromosomal regions were categorized as suppressors. Interestingly, 4 deficiency lines in cytogenetic map region 87 suppressed the cycle 14 phenotype: *Df(3R)ry615*, *Df(3R)kar-Sz8*, *Df(3R)kar-Sz21*, and *Df(3R)ry614* (Figure 3 and Table 1). Each of the following eight suppressors comes from an independent chromosomal region: *Df(1)B*, *Df(2L)spd$^{j2}$*, *Df(2L)J77*, *Df(2R)cn9*, *Df(3L)R-G5*, *Df(3L)vin7*, *Df(3L)fz-GS1a*, and *Df(3R)crb87-4* (Figure 3, Table 1).

We have concentrated our investigation on suppressors because they are less prone to false positives than are enhancers. Identification of gene products within

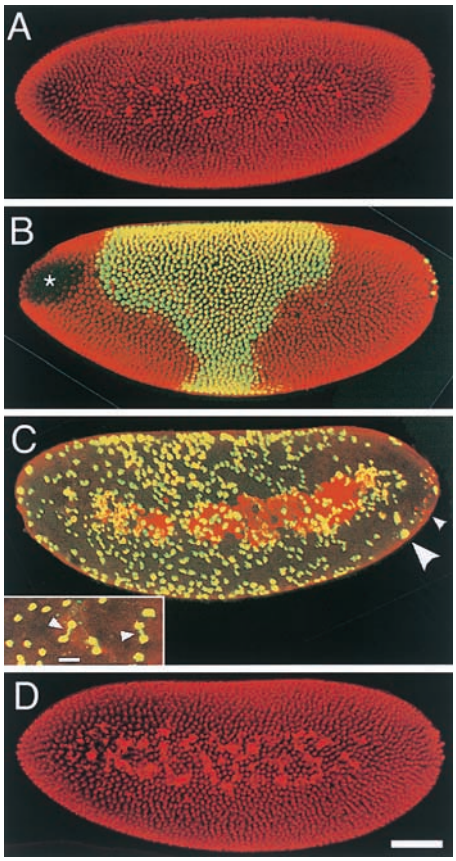


Figure 2.—Nuclear morphology at cycle 14. Embryos were stained with antihistone H1 (red) and anti-phospho-histone H3 (green) to detect nuclei in mitosis (merged in yellow); anterior is to the left. (A) Wild-type embryo: In cycle 14 nuclei do not divide for at last 60 min. (B) *Six cycB* embryo: note uneven distribution (*, area of no nuclei) and a patch of nuclei in mitosis (yellow). (C) *Df(2L)TW84/six cycB* embryo is an example of an enhancer line. The more severe cycle 14 phenotype is obvious: many nuclei are in mitoses (yellow) and many yolk nuclei in the center are not in mitosis (red). Also, nuclei are unevenly distributed, and we observed chromosomal bridges (inset shows a close-up view in which arrowheads indicate chromosomal bridges; bar, 10 μm), macronuclei (large arrowhead), and micronuclei (small arrowhead). (D) *Df(3R)ry614/six cycB* is an example of a suppressor line with only normal interphase nuclei; bar, 65 μm. Images are projections of 18–20 optical sections with a 2.5-μm interval.

the interacting deficiencies led us to find gene products involved in three biological processes: cell-cycle control and microfilament and microtubule modification.

**Two suppressors normalized both astral microtubule morphology and Cdk1-CycB activity during cycles 5–7:** The obvious question is how the cycle 14 phenotype is normalized in the suppressor lines. One possibility is that the suppression at cycle 14 results from normalization of Cdk1-CycB activity and microtubule morphology at earlier cycles, which could account for rescuing all later stages up to cycle 14. Cdk1 activity during cycles 5–7 is defined by maternal CycB levels (Stiffler *et al.* 1999). Compared to wild-type embryos, the Cdk1-CycB activity is significantly higher in *six cycB* embryos (Figure 4D, Table 3). Higher Cdk1 activity causes shorter microtubules while lower Cdk1 activity correlates with longer microtubules (Stiffler *et al.* 1999; Figures 1 and 4) and an abnormal cycle 10 phenotype (Figures 1 and 5). Using the frequency of metaphase spindles with asters as an indicator of the microtubule morphology, we found that in wild-type embryos, 84% of metaphase spindles have astral microtubules, while in *six cycB* embryos this percentage is significantly lower (60%; Figure 4 and Table 3). Conversely, in embryos with one copy of maternal *cycB* (*one cycB* embryos), Cdk1 activity during cycles 5–7 is lower than that in wild-type controls (Stiffler *et al.* 1999), and we observed a higher frequency of metaphase spindles with astral microtubules (99%, Table 3). Thus, we tested whether suppressors normalize the *six cycB* phenotype before cycle 10 by analyzing metaphase astral microtubule morphology and Cdk1-CycB activity during cycles 5–7 in all suppressor *Df/six cycB* embryos.

The suppressor deficiency line *Df(3R)ry615* covers the other three suppressor deficiencies in region 87 (Figure 3, Table 1). In *Df(3R)ry615/six cycB* embryos, the frequencies of metaphase spindle with asters were normalized significantly compared to *six cycB* embryos (Figure 4, Table 3). We also found that *Df(3R)ry615/six cycB* embryos had ~20% less Cdk1-CycB kinase activity than that of the *six cycB* embryos (Table 3) and that these embryos had normal nuclear distribution at cycle 10 (data not shown). We made similar observations with *Df(2L)J77* in cytogenetic map region 31 (Table 3). The restoration of the astral microtubule morphology and the reduced Cdk1 activity caused by loss of genes in both regions 87 and 31 suggest that their products regulate microtubule stability and/or Cdk1-CycB activity. Normalization of microtubules was already evident at cycles 5–7 and might account for the normal development later at cycles 10 and 14.

For suppressor lines in the remaining seven chromosomal regions, neither the astral microtubule morphology nor the Cdk1 activity was improved over that of *six cycB* embryos (data not shown). Further observations of live embryos and fixed materials showed no differences at cycle 10 compared to *six cycB* embryos (data not shown). Therefore, these seven suppressors must rescue the *six cycB* phenotype between cycles 10 and 14.

As we show below, the observation that the suppressor deficiency lines can restore the astral microtubule morphology and Cdk1-CycB activity led to the identification of *cdk1*, *cycA*, and *Arp87C* as suppressor genes within the previously identified deficiencies.

***Df(2L)J77* implicates *cdk1* as a suppressor of the *six cycB* phenotype:** The suppressor *Df(2L)J77* (at cytogenetic map region 31C; 31E7) covers the *cdk1* gene (at 31D11; Clegg *et al.* 1993). To directly test whether loss of *cdk1* suppresses the *six cycB* phenotype, we measured Cdk1-CycB activities in $cdk1^{D57}$*/six cycB* embryos. The

**TABLE 1**

**Deficiency lines that enhance or suppress the cycle 14 phenotype of *six cycB* embryos**

| Maternal genotype | Cytogenetic breakpoints | *two cycB* background | | | *six cycB* background | | |
|---|---|---|---|---|---|---|---|
| | | Normal cycle 14 embryos (%) | 95% C.I. (%)[a] | $N^b$ | Normal cycle 14 embryos (%) | 95% C.I. (%)[a] | $N^b$ |
| Wild type | | 97 | 95–98 | 409 | | | |
| *six cycB* | | | | | 74 | 71–77 | 790 |
| | | Enhancer deficiencies | | | | | |
| *Df(1)N19* | 17A1; 18A2 | 95 | 89–98 | 101 | 19 | 13–26 | 155 |
| *Df(2L)GpdhA*[c] | 25D7; 26A8–9 | 69 | 52–82 | 35 | 4 | 0–19 | 24 |
| *Df(2L)TW84* | 38A1; 39D3–E1 | 75 | 68–81 | 181 | 18 | 11–26 | 113 |
| *Df(2L)TW161* | 38A6; 40A4–B1 | 88 | 81–94 | 102 | 13 | 5–26 | 39 |
| *Df(2L)TW1* | 38A7–B1; 39C2–3 | 96 | 92–99 | 133 | 15 | 11–20 | 278 |
| *Df(2L)DS6* | 38E2; 39E7 | 93 | 88–96 | 193 | 20 | 13–28 | 110 |
| *Df(2R)Pcl7B* | 54E8–F1; 55B9–C1 | 96 | 89–98 | 89 | 14 | 5–31 | 28 |
| *Df(2R)PC4* | 55A1; 55F1–2 | 93 | 88–97 | 135 | 0 | 0–6 | 52 |
| *Df(2R)Pcl11B* | 55A1; 55C1–3 | 74 | 66–80 | 160 | 15 | 8–26 | 60 |
| *Df(2R)AA21* | 56F9–11; 57D12 | 84 | 76–90 | 108 | 17 | 11–25 | 101 |
| *Df(3L)Ar14-8* | 61C4; 62A8 | 93 | 87–96 | 138 | 16 | 9–26 | 70 |
| *Df(3L)fz-GF3b* | 70C2; 70D5 | 78 | 72–84 | 181 | 3 | 1–9 | 74 |
| *Df(3L)fz-M21* | 70D2; 71E4–5 | 90 | 83–95 | 92 | 10 | 4–22 | 48 |
| | | Suppressor deficiencies | | | | | |
| *Df(1)B* | 15F1–2;16A7 | 100 | 98–100 | 153 | 89* | 74–96 | 35 |
| *Df(2L)spd*$^{j2}$ | 27B2; 27F1–2 | 93 | 87–97 | 112 | 93* | 86–97 | 86 |
| *Df(2L)J77* | 31C; 31E7 | 89 | 83–94 | 148 | 86* | 79–92 | 107 |
| *Df(2R)cn9* | 42E; 44C1 | 100 | 94–100 | 54 | 92* | 74–99 | 24 |
| *Df(3L)R-G5* | 62A10–B1; 62C4–D1 | 93 | 90–95 | 326 | 83* | 76–88 | 161 |
| *Df(3L)vin7* | 68C8; 69B4–5 | 92 | 85–96 | 120 | 85* | 75–93 | 67 |
| *Df(3L)fz-GS1a* | 70D2; 70E4–5 | 97 | 92–99 | 95 | 92* | 82–97 | 52 |
| *Df(3R)ry615* | 87B12; 87E8 | 91 | 87–94 | 213 | 81* | 77–85 | 392 |
| *Df(3R)kar-Sz8* | 87C1–2; 87E14 | 99 | 96–100 | 117 | 84* | 76–89 | 117 |
| *Df(3R)kar-Sz21* | 87C7; 87C8–9 | 100 | 88–100 | 25 | 95* | 89–98 | 87 |
| *Df(3R)ry614* | 87D2–4; 87D14 | 98 | 95–99 | 191 | 96* | 92–98 | 131 |
| *Df(3R)crb87-4* | 95D11–E2; 96A2 | 76 | 69–82 | 180 | 95* | 88–98 | 79 |

*The percentage of normal embryos is significantly higher than that of *six cycB* embryos (Pearson's chi-square test, $P < 0.03$).
[a] The Blyth-Still-Casella 95% confidence interval (C.I.) for the percentage of normal cycle 14 embryos.
[b] Number of embryos analyzed.
[c] Additional deficiency lines covering these regions are not enhancers.

Cdk1$^{D57}$ protein has a single-amino-acid change within the catalytic core of the enzyme. Therefore, the Cdk1$^{D57}$ protein may stably bind with CycB but the resulting complex would have no kinase activity. If this is occurring, the Cdk1$^{D57}$ protein may actively titrate out CycB since *cdk1*$^{D57}$ is considered as an antimorphic allele (Clegg *et al.* 1993; Stern *et al.* 1993). We found that in *cdk1*$^{D57}$*/six cycB* embryos, Cdk1-CycB activity is significantly reduced compared to *six cycB* embryos (Table 3). In addition, microtubule morphology is also normalized in *cdk1*$^{D57}$*/six cycB* embryos (Table 3). We tested other *cdk1* alleles, *cdk1*$^{B47}$ (null), *cdk1*$^{216P}$, and *cdk1*$^{E1\text{-}24}$ (hypomorph). However, unlike *cdk1*$^{D57}$, these alleles did not improve the hatching rates in the *six cycB* background embryos. The observation that the *Df(2L)J77* and the neomorphic allele *cdk1*$^{D57}$ but not the null allele of *cdk1* reduce kinase activity of the *six cycB* embryo indicates that there is another gene within *Df(2L)J77* whose product interacts with Cdk1.

In wild-type embryos, Cdk1 is not likely to be limiting for kinase activity in preblastoderm cycles for two reasons: First, the inhibitory phosphates on Cdk1 (Thr14 and Tyr15) are not detected in these early cycles (Edgar *et al.* 1994). Second, Cdk1-CycB activity is higher in *four cycB* embryos compared to wild-type embryos (Stiffler *et al.* 1999). However, the observation that Cdk1-CycB activity is lower in *cdk1*$^{D57}$*/six cycB* embryos compared to *six cycB* embryos indicates that Cdk1 becomes limiting in *six cycB* embryos. Thus, reducing Cdk1-CycB activity in the *cdk1*$^{D57}$*/six cycB* embryos may normalize microtubule morphology at cycles 5–7 and account for the rescue at both cycles 10 and 14 (Table 4, class I).

***Df(3L)vin7* implicates *cycA* as a suppressor of the *six cycB* phenotype:** Since Cdk1-CycB plays a pivotal role in regulating cell-cycle progression, its activity is under tight control of several gene products (Morgan 1995). We tested specific genes whose products are known to regulate Cdk1 activity. In particular we were interested

**TABLE 2**

**Specific genes that suppress the cycle 14 phenotype of the *six cycB* embryos**

| | *two cycB* background | | | *six cycB* background | | |
|---|---|---|---|---|---|---|
| Mutant | Normal cycle 14 embryos (%) | 95% C.I. (%)[a] | $N^b$ | Normal cycle 14 embryos (%) | 95% C.I. (%)[a] | $N^b$ |
| Wild type | 97 | 95–98 | 409 | | | |
| *six cycB* | | | | 74 | 71–77 | 790 |
| | | | Cdk1 regulating genes | | | |
| $cdk1^{D57}$ | 98 | 94–100 | 109 | 90* | 87–93 | 450 |
| $cycA^{neo114}$ | 92 | 87–95 | 199 | 90* | 86–93 | 307 |
| $cycA^{C8LR1}$ | 96 | 92–98 | 155 | 85* | 81–88 | 442 |
| | | | Microtubule-microfilament interacting genes | | | |
| *Arp87C* | 97 | 94–99 | 272 | 68 | 64–72 | 490 |
| $dmn^{K16109}$ | 99 | 97–100 | 205 | 69 | 61–77 | 139 |
| | | | Microfilament regulating/interacting genes | | | |
| $chic^{8893}$ | 99 | 96–100 | 122 | 98* | 96–99 | 313 |
| $chic^{4205}$ | 99 | 96–100 | 124 | 94* | 90–96 | 226 |
| $chic^{7772}$ | 100 | 97–100 | 135 | 91* | 88–94 | 398 |
| $chic^{7886}$ | 100 | 99–100 | 272 | 90* | 85–93 | 256 |
| $chic^{0135}$ | 99 | 96–100 | 157 | 70 | 63–76 | 196 |
| $chic^{0281}$ | 97 | 88–99 | 55 | 62 | 54–70 | 137 |
| $dia^{1}$ | 94 | 90–96 | 242 | 96* | 94–97 | 445 |
| $dia^{2}$ | 98 | 95–99 | 241 | 93* | 87–96 | 136 |
| $dia^{9}$ | 98 | 94–99 | 125 | 90* | 88–92 | 634 |
| $Cdc42^{2}$ | 82 | 75–88 | 141 | 93* | 90–95 | 352 |
| $Cdc42^{4}$ | 86 | 79–92 | 110 | 79 | 72–84 | 179 |
| $qua^{HM14}$ | 99 | 97–100 | 329 | 95* | 91–98 | 163 |
| $qua^{PX42}$ | 98 | 94–99 | 145 | 97* | 95–98 | 328 |
| $qua^{WP165}$ | 94 | 89–97 | 154 | 66 | 61–70 | 447 |
| $sqh^{1}$ | 93 | 89–96 | 191 | 90* | 83–94 | 140 |
| $sqh^{2}$ | 86 | 79–91 | 127 | 69 | 64–73 | 434 |
| $zip^{1}$ | 97 | 94–98 | 294 | 85* | 79–90 | 193 |
| $sced^{1}$ | 94 | 86–98 | 70 | 91* | 78–97 | 42 |

*The percentage of normal embryos is significantly higher than that of *six cycB* embryos (Pearson's chi-square test, $P < 0.03$).

[a] The Blyth-Still-Casella 95% confidence interval (C.I.) for the percentage of normal cycle 14 embryos.

[b] Number of embryos analyzed.

in *cycA* (at cytogenetic map position 68E1), which lies within the region defined by suppressor *Df(3L)vin7* (68C8; 69B4–5). Reducing CycA (with both the hypomorphic allele $cycA^{neo114}$ and the null allele $cycA^{C8LR1}$) rescued the *six cycB* cycle 14 phenotype (Table 2) and restored astral microtubule morphology (Table 3), but did not alter the Cdk1-CycB activity (Table 3). Both Cdk1-CycA and Cdk1-CycB are able to regulate microtubule dynamics as shown in Xenopus egg extracts (Verde *et al.* 1992). Thus reducing CycA may stabilize microtubule morphology without affecting Cdk1-CycB activity.

We tested a number of additional known regulators of Cdk1-CycB that were not implicated by the deficiency screen for their ability to suppress the *six cycB* phenotype, for example, *cyclin B3* ($cycB3^{2}$ and $cycB3^{3}$, at cytogenetic map position 96B1), *Dwee1* ($Dwee^{DS1}$ and $Dwee^{ES1}$, at 27B3), *grapes* ($grp^{1}$, at 36A10), *Regulator of cyclin A1* ($Rca1^{11294}$, at 27C1), *string* ($stg^{1}$, at 99A5), and *twine* ($twe^{1}$, at 35F1). These genes neither suppressed nor enhanced the *six cycB* phenotype at cycle 14 (data not shown).

***Df(3R)ry615* implicates *Arp87C* as a suppressor of the *six cycB* phenotype:** Since one aspect of suppression was restoration of astral microtubule morphology, we tested genes whose products might affect microtubule dynamics. We concentrated on chromosomal region 87, where we identified four suppressor deficiency lines. We specifically tested two deficiency lines, *Df(3R)ry615* and *Df(3R)kar-Sz21*, for microtubule morphology and only *Df(3R)ry615* for Cdk1-CycB activity. Both the microtubule morphology and Cdk1 activity were normalized in these two lines (Table 3). One candidate gene in this region is *Arp87C* (actin-related protein 87C, also known as *arp1* or *gridlock*, localized at cytogenetic map position 87C5; Fyrberg *et al.* 1994; Haghnia *et al.* 2001). Arp1 protein is a key component of the dynactin complex, which is composed of 10 well-characterized subunits, such as p150/Glued, p50/Dynamitin, p62, and capping proteins (Schroer *et al.* 1996). We tested whether *Arp87C* was responsible for the suppression observed in *Df(3R)ry615* and *Df(3R)kar-Sz8* and indeed found that

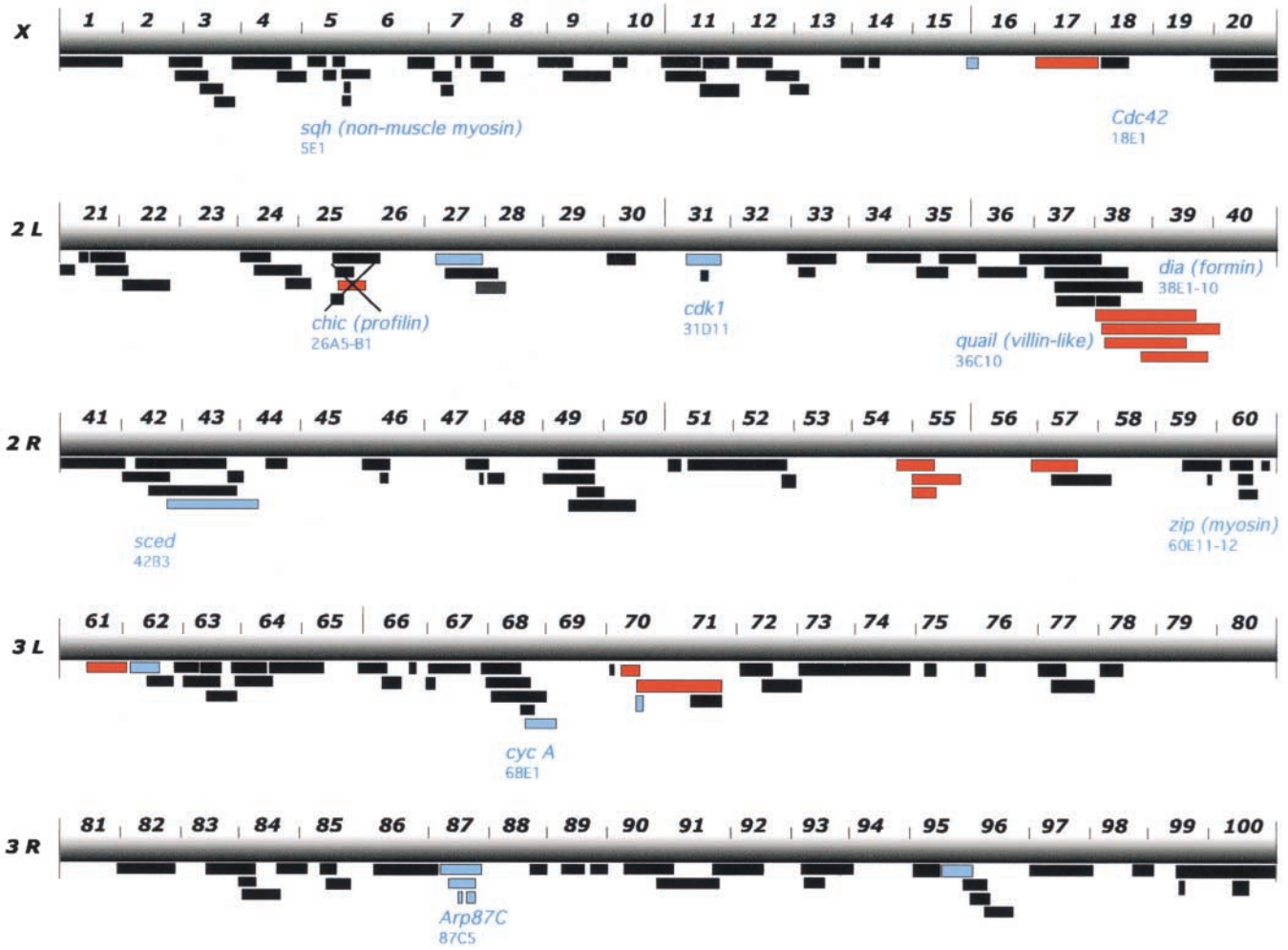


FIGURE 3.—Cytogenetic map of salivary gland polytene chromosome of deficiencies tested for enhancement or suppression of the *six cycB* phenotype. The Drosophila genome is subdivided into 100 salivary gland units, 20 units per chromosome arm (X, 2L, 2R, 3L, and 3R). The relative position of all tested deficiencies is shown. Black bars indicate no enhancement or suppression. Enhancing deficiencies are shown in red and suppressor deficiencies in blue. We identified 12 enhancing deficiency lines and 12 suppressing deficiency lines (see Table 1 for details). The 10 specific suppressor genes identified are as follows: *Actin-related protein 87C* (*Arp87C*), *Cdc42*, *chickadee* (*chic*), *cyclin A* (*cycA*), *cyclin-dependent kinase 1* (*cdk1*), *diaphanous* (*dia*), *quail* (*qua*), *scrambled* (*sced*), *spaghetti-squash* (*sqh*), and *zipper* (*zip*).

astral microtubule morphology was restored and that Cdk1-CycB activity was reduced in *Arp87C/six cycB* embryos in cycles 5–7 (Figure 4, C and D; Table 3). However, *Arp87C/six cycB* embryos showed similar cycle 14 phenotypes to *six cycB* embryos (Table 2), indicating that restoration of microtubule organization before cycle 10 did not always guarantee a normal cycle 14 phenotype (Table 4, class II).

We also tested *p150/Glued* (*Gl*, at cytogenetic map position 70C5–6) and *p50/dynamitin* (*dmn*, at 44F3), two components of the dynactin complex, by using the dominant negative allele $Gl^{1}$ (SWAROOP *et al.* 1985) and the hypomorphic allele $dmn^{K1610}$. We found that compared to *six cycB* embryos, reducing *Gl* rescued the astral microtubule morphology at cycles 5–7, which is similar to reducing *Arp87C* (Table 3). We further tested dynein light chain *roadblock* (*robl*, at 54B16) using the null allele $robl^{K}$ and dynein heavy chain (*Dhc*, at 64C1–2) using the null allele $Dhc^{4-19}$ and hypomorphic allele $Dhc^{6-10}$. These two proteins are components of the dynein complex. Surprisingly, reducing either *Dhc* or *robl* led to significantly shorter astral microtubules than in *six cycB* embryos (Table 3). These observations suggest that the dynein complex and the dynactin complex may have different effects on astral microtubule morphology.

**Mutations in genes that regulate microfilament networks can suppress the *six cycB* phenotype:** In Drosophila, ~80 proteins bind with actin and regulate microfilament stability in addition to the myosin motor superfamily and proteins that interact with the motor subunits (GOLDSTEIN and GUNAWARDENA 2000). The dynactin complex interacts with both microtubules and microfilaments (SCHROER *et al.* 1996; GARCES *et al.* 1999; see DISCUSSION). The observation that reducing *Arp87C*

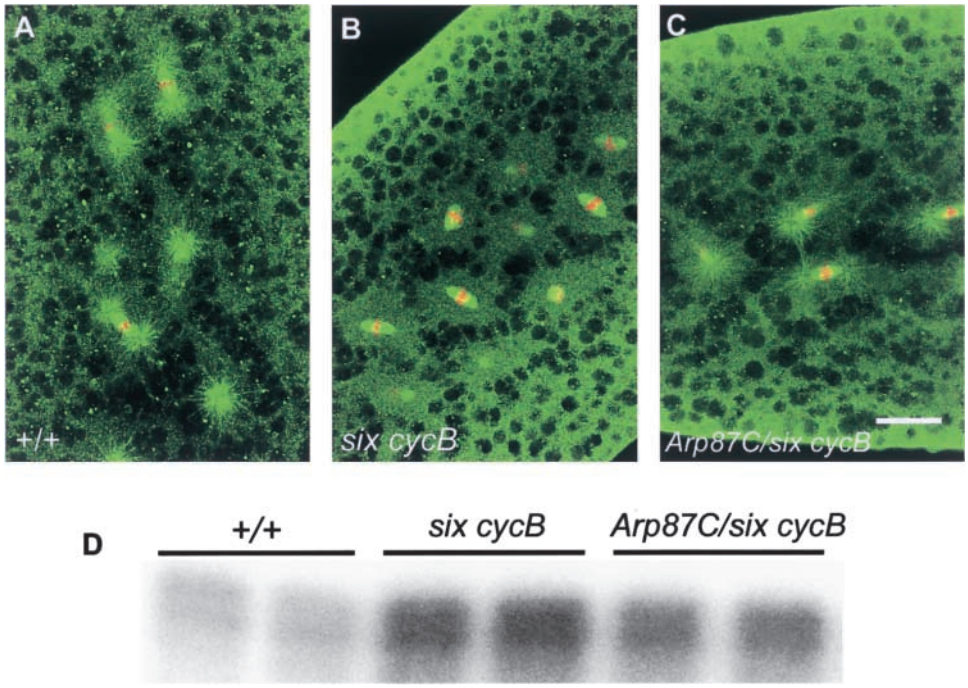


FIGURE 4.—Metaphase astral microtubule morphology in embryos at cycle 6 (A–C) and Cdk1-CycB kinase assay of embryos at cycles 5–7 (D). Cycle 6 metaphase embryos were stained with polyclonal anti-phospho-histone H3 (red) and monoclonal anti-tubulin (green) antibodies. Images are single optical sections. (A) Wild-type embryo. (B) *six cycB* embryo with reduced astral microtubules. (C) *Arp87C/six cycB* embryo with a normalized phenotype. Bar, 30 μm. (D) One example of Cdk1-CycB kinase assay, composed two independent samples of wild-type and *six cycB* embryos and two samples of *Arp87C/six cycB* embryos.

suppressed the *six cycB* phenotype led us to ask whether some of the microfilament regulatory proteins have an effect on microtubule stability and/or Cdk1-CycB activity.

We tested *chickadee* (*chic*, at cytogenetic map position 26A5–B1) for suppression of the *six cycB* phenotypes even though it was not isolated from the deficiency screen, because loss of *chic* leads to more stable microtubules in the Drosophila egg chambers (MANSEAU *et al.* 1996). The stabilized microtubule may in turn lead to more CycB degradation (see DISCUSSION). The gene *chic* encodes the Drosophila homolog of profilin (COOLEY *et al.* 1992). Different alleles can have different amino acid changes, which could generate very different phenotypes. Thus, to interpret the function of a gene product, it is important to use different alleles when possible. Reducing profilin by using any of the four hypomorphic *chic* alleles ($chic^{8893}$, $chic^{4205}$, $chic^{7772}$, and $chic^{7886}$) in a *six cycB* background resulted in a significantly higher percentage of normal cycle 14 embryos compared to *six cycB* embryos (Table 2). The hypomorphic $chic^{0135}$ and the null allele $chic^{0281}$, however, did not suppress the *six cycB* cycle 14 phenotype (Table 2).

To rule out the possibility that the allelic difference was caused by the genetic background, we outcrossed the $chic^{0135}$-carrying chromosome with a multiply marked chromosome and replaced 60% of the $chic^{0135}$ chromosome. Since replacing the genetic background of the $chic^{0135}$ did not rescue the cycle 14 phenotype, the results appeared to be allele specific. The alleles $chic^{0135}$ and $chic^{7886}$ are *P*-element insertions in the first exon at exactly the same site and orientation, but lead to different phenotypes: While both alleles produce weakly fertile females, only $chic^{0135}$ is male sterile (L. COOLEY, personal communication). The phenotypic difference between the two alleles is not clear and may be caused by some other lesion in the nonrecombined region of the $chic^{0135}$ genome or by an internal deletion in the *P* element of $chic^{0135}$ or $chic^{7886}$.

Interestingly, looking at astral microtubule morphology in cycle 5–7 embryos, we found that all alleles of *chic*, with the exception of the null allele $chic^{0281}$, restored microtubule morphology to different degrees (Table 3). We then specifically tested Cdk1-CycB activity in $chic^{7886}$/*six cycB* embryos and found that Cdk1-CycB activity was significantly reduced compared to that of *six cycB* embryos (Table 3). Therefore, the hypomorphic alleles of *chic* restored astral microtubule morphology and this correlates with a normal cycle 10 and 14 phenotype (Table 4, class I).

In many organisms, profilin is found to bind with Formin homology (FH) proteins, which play important roles in coordinating cytokinesis (WASSERMAN 1998). In *Saccharomyces cerevisiae*, the FH protein Bni1p binds with profilin and the activated form of the Rho family protein GTPase Cdc42p (EVANGELISTA *et al.* 1997). In Drosophila, there are two FH proteins, Diaphanous (Dia) and Cappuccino (Capu), both of which have been shown to bind with Chic (profilin; CASTRILLON and WASSERMAN 1994; MANSEAU *et al.* 1996), but it is not clear if Chic, Dia, and Cdc42 function in a complex in Drosophila. Since we already identified *chic* as a suppressor, we tested *capu* (at cytogenetic map position 24C8–9), *dia* (at 38E5–6), and *Cdc42* (at 18E1) for suppression of *six cycB* phenotypes even though these regions did not act as suppressors in our initial deficiency screen.

**TABLE 3**

**Characterization of suppressor deficiency lines and suppressor genes with respect to metaphase astral microtubule morphology and Cdk1-CycB activities between cycles 5 and 7**

| Maternal genotype | Metaphase spindles with asters (%) | $N^a$ | Cdk1-CycB activity (SD) | $N^b$ |
|---|---|---|---|---|
| Wild type | 84 | 63 | 56.9 (13.6)**** | 42 |
| *six cycB* | 60* | 68 | 100.0 | 42 |
| *one cycB* | 99* | 17 | 34.1[c] | |
| | Deficiencies | | | |
| *Df(3R)ry615/six cycB* | 84** | 10 | 81.6 (5.5)**** | 8 |
| *Df(3R)kar-Sz21/six cycB* | 90** | 16 | ND[d] | |
| *Df(2L)J77/six cycB* | 81** | 18 | 82.5 (15.2)**** | 12 |
| | Cdk1 regulating genes | | | |
| *cdk1$^{D57}$/six cycB* | 84** | 35 | 72.3 (14.7)**** | 10 |
| *cycA$^{neo114}$/six cycB* | 75** | 23 | ND | |
| *cycA$^{C8LR1}$/six cycB* | 84** | 16 | 104.7 (2.3) | 4 |
| | Microtubule-microfilament interacting genes | | | |
| *Arp87C/six cycB* | 80** | 52 | 73.1 (8.6)**** | 8 |
| *dmn$^{K16109}$/six cycB* | 54 | 44 | 96.5 (23.3) | 6 |
| *Gl$^{l}$/six cycB* | 81** | 19 | ND | |
| *Dhc$^{4-19}$/six cycB* | 26*** | 28 | ND | |
| *Dhc$^{6-10}$/six cycB* | 48*** | 42 | ND | |
| *robl$^{K}$/six cycB* | 34*** | 29 | ND | |
| | Microfilament regulating/interacting genes | | | |
| *chic$^{8893}$/six cycB* | 80** | 9 | ND | |
| *chic$^{4205}$/six cycB* | 87** | 10 | ND | |
| *chic$^{7772}$/six cycB* | 70 | 27 | ND | |
| *chic$^{7886}$/six cycB* | 85** | 22 | 88.7 (5.6)**** | 10 |
| *chic$^{0135}$/six cycB* | 70 | 15 | ND | |
| *chic$^{0281}$/six cycB* | 63 | 23 | ND | |
| *dia$^{1}$/six cycB* | 65 | 21 | ND | |
| *dia$^{2}$/six cycB* | 58 | 56 | 94.0 (5.6) | 10 |
| *dia$^{9}$/six cycB* | 69 | 29 | ND | |
| *Cdc42$^{2}$/six cycB* | 40 | 21 | 94.4 (10.5) | 8 |
| *qua$^{HM14}$/six cycB* | 71 | 30 | ND | |
| *qua$^{PX42}$/six cycB* | 94** | 10 | ND | |
| *qua$^{WP165}$/six cycB* | 81** | 17 | 70.5 (8.0)**** | 6 |
| *sqh$^{1}$/six cycB* | 75** | 27 | 93.7 (22.3) | 10 |
| *sqh$^{2}$/six cycB* | 76 | 23 | 99.9 (10.5) | 4 |
| *zip$^{1}$/six cycB* | 70 | 18 | 141.8 (62.9) | 6 |
| *sced$^{1}$/six cycB* | 84** | 39 | 88.5 (5.5)**** | 8 |

*Significantly different from wild-type embryos with the one-sided Wilcoxon-Mann-Whitney test; **significantly higher than *six cycB* embryos with the one-sided Wilcoxon-Mann-Whitney test; ***significantly lower than *six cycB* embryos with the one-sided Wilcoxon-Mann-Whitney test; ****significantly lower than *six cycB* embryos with both the one-sample *t*-test and the Wilcoxon signed-rank test for one-sample data.

[a] Number of metaphase embryos analyzed for astral microtubule morphology.

[b] Number of independent samples of each genotype for Cdk1-CycB kinase assay.

[c] This is relative Cdk1 activity based on results that Cdk1-CycB activity in *one cycB* embryos is ~60% of the wild-type embryos (Stiffler *et al.* 1999).

[d] ND, not determined.

Similar to the suppressing effect of the *chic* alleles, we found that the hypomorphic alleles *dia$^{1}$*, *dia$^{9}$*, *Cdc42$^{2}$*, and null allele *dia$^{2}$* (Castrillon and Wasserman 1994; Genova *et al.* 2000) indeed suppressed the *six cycB* cycle 14 phenotype (Table 2). However, *capu$^{RK12}$* and the null allele *Cdc42$^{4}$* neither suppressed nor enhanced the *six cycB* cycle 14 phenotype (Table 2 and data not shown). In contrast to *chic*, both astral microtubule morphology and Cdk1-CycB activity were not normalized in *dia/six cycB* or *Cdc42/six cycB* embryos during cycles 5–7 (Table 3), suggesting that they do not affect microtubule stability before cycle 10. This indicates that suppression of the cycle 14 phenotype can be independent of an earlier suppression (Table 4, class III). This observation is similar to the majority of suppressor deficiency lines.

The identification of *chic*, *dia*, and *Cdc42* as suppres-

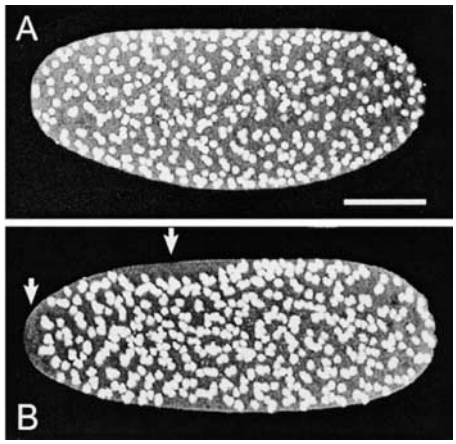


FIGURE 5.—Cycle 10 phenotype of fixed embryos: (A) wild-type embryo and (B) *six cycB* embryo. Note that in the *six cycB* embryo, some nuclei have not yet reached the cortex in the anterior and anterior-medial regions (arrows). These images are midsagittal optical sections and embryos are oriented as anterior to the left and dorsal up. Bar, 100 μm.

sors encouraged us to test more genes whose products can regulate microfilament dynamics or interact with microfilaments. Although the corresponding deficiencies did not act as suppressors in our screen, we identified alleles of *quail* (*qua*, encodes villin-like protein, at cytogenetic map position 36C10), *spaghetti-squash* (*sqh*, encodes cytoplasmic myosin II regulatory light chain, at 5E1), *zipper* (*zip*, encodes nonmuscle myosin heavy chain, at 60E11–12), and *scrambled* (*sced*, at 42B3) as suppressors of the *six cycB* cycle 14 phenotype (Figure 3, Table 2).

Specifically, $qua^{HM14}$ and $qua^{PX42}$ suppressed the *six cycB* cycle 14 phenotype while $qua^{WP165}$ did not (Table 2). $qua^{HM14}$ and $qua^{WP165}$ are weak hypomorphic alleles, whereas $qua^{PX42}$ is a strong hypomorphic allele (MAHAJAN-MIKLOS and COOLEY 1994). At cycles 5–7, the astral microtubule morphology was restored in $qua^{PX42}$/*six cycB* and $qua^{WP165}$/*six cycB* embryos but not in $qua^{HM14}$/*six cycB* embryos (Table 3). The hypomorphic allele $sqh^{1}$ suppressed the cycle 14 phenotypes (Table 2) and microtubule morphology at cycles 5–7 was restored *in* $sqh^{1}$/*six cycB* and $sqh^{2}$/*six cycB* embryos, but Cdk1-CycB activities were not significantly reduced (Table 3). The amorphic allele $zip^{1}$ suppressed the cycle 14 phenotype but not microtubule morphology and Cdk1-CycB activity at cycles 5–7 (Tables 2 and 3). The null allele $sced^{1}$ in the *six cycB* background also suppressed the *six cycB* cycle 14 phenotype (Table 2), restored astral microtubule morphology, and reduced Cdk1 activity at cycles 5–7 (Table 3). Sced has been shown to be involved in regulating nuclear migration and cytokinesis (STEVENSON *et al.* 2001).

Reducing any of these four gene products (Qua, Sqh, Zip, and Sced) may weaken the microfilament network by reducing either the contractility of the microfilament network or the microfilament stability. If this interpretation is correct, weakening of the microfilament network may strengthen microtubule stability (see DISCUSSION).

We also tested $Merlin^{3}$ (at cytogenetic map position 18E1), *peanut* ($pnut^{02502}$ and $pnut^{XP}$, at 44C1), $scraps^{8}$ (at 43E3), α-$Spectrin^{rg41}$ (at 62B–4), β-$Spectrin^{emb}$ (at 16B12–C1), and $\beta_{Heavy}$-*Spectrin* (at 63D2). None of these genes altered the *six cycB* cycle 14 phenotype (data not shown) despite the fact that products of some of them (*Pnut*, α-*Spec*, β-*Spec*, $\beta_H$-*Spec*) bind with both microtubules and microfilaments in Drosophila (SISSON *et al.* 2000).

**Axial expansion is normalized during cycles 4–7 in *chic/six cycB* embryos:** Because axial expansion and cortical migration depend on proper microtubule and microfilament dynamics, we predicted that suppressors that normalize microtubule morphology at cycles 5–7 also normalize nuclear migration. We previously reported that during the axial expansion cycles the energids (nuclei and surrounding cytoplasm) of *four cycB* embryos migrate significantly slower than those of wild-type controls (STIFFLER *et al.* 1999). To test whether reducing Chic or Dia normalizes nuclear migration, we measured the velocity of migrating energids in *six cycB*, $chic^{7886}$/*six cycB*, and $dia^{2}$/*six cycB* embryos. Energids in *six cycB* embryos migrated at a rate of 8.9 μm/min ($N = 12$), which was slower than those in both wild-type (14.5

**TABLE 4**

**Summary of suppression of the *six cycB* phenotypes at different developmental stages**

| Class | Maternal genotype | Cycles 5–7 | | Cycle 10 | Cycle 14 |
|---|---|---|---|---|---|
| | | Astral microtubule morphology | Cdk1-CycB activity | | |
| I | $cdk1^{D57}$/*six cycB* | Yes | Yes | Yes | Yes |
| I | $chic^{7886}$/*six cycB* | Yes | Yes | Yes | Yes |
| I | $qua^{WP165}$/*six cycB* | Yes | Yes | Yes | Yes |
| I | $sced^{1}$/*six cycB* | Yes | Yes | Yes | Yes |
| II | *Arp87C/six cycB* | Yes | Yes | Yes | No |
| III | $dia^{2}$/*six cycB* | No | No | No | Yes |
| III | $Cdc42^{2}$/*six cycB* | No | No | No | Yes |
| III | $zip^{1}$/*six cycB* | No | No | No | Yes |

μm/min) and *four cycB* (13.0 μm/min) embryos (Stiffler *et al.* 1999). The velocity of energids in *chic$^{7886}$/six cycB* embryos was 13.4 μm/min ($N = 10$), which was improved toward the wild-type rate and was significantly faster than that in *six cycB* embryos ($P = 0.0004$). Compared to those of *six cycB* embryos, energids migrated even slower in *dia$^{2}$/six cycB* embryos (6.3 μm/min, $N = 4$). This observation is consistent with the idea that lowering the amount of Chic protein normalizes microtubule morphology and therefore nuclei migrate faster than those of the *six cycB* embryos, while lowering Dia has no effect on microtubules and therefore velocity of nuclear movement is not normalized.

We also analyzed the number and duration of axial expansion cycles in wild-type, *six cycB*, and *chic$^{7886}$/six cycB* embryos. *Six cycB* embryos often had one more axial expansion cycle than controls, and nuclei moved slightly but for a significantly longer time (5.6 min) compared to controls (5.3 min). Compared with *six cycB* embryos, *chic$^{7886}$/six cycB* embryos had normal nuclear movement in terms of both the numbers of axial expansion cycles and the duration of nuclear movement (5.1 min).

**Somatic bud formation is normalized during cycles 9–10 and cycle 10 phenotype analyses in the *six cycB* embryos:** Cortical migration of nuclei depends on microtubule function (Baker *et al.* 1993). Nuclei first penetrate the cortex at the posterior pole at cycle 9, and then at cycle 10 all somatic buds appear and pole cells are formed (Foe and Alberts 1983). Live analysis of wild-type embryos revealed that all somatic buds appear at the cortex within 2 min (1.3 min, $N = 13$, SD = 0.5). However, in *six cycB* embryos, it takes longer (12.8 min, $N = 14$, SD = 8.0) and more than one cycle until all somatic buds appear at the surface. In contrast, somatic bud formation in *chic$^{7886}$/six cycB* embryos is completed within 3.8 min ($N = 13$, SD = 2.5), which is significantly faster than that in *six cycB* but is slower than that in controls.

This uneven migration pattern was also observed in fixed embryos. Wild-type embryos fixed at cycle 10 had nuclei evenly distributed at the cortex in 97% ($N = 97$) of the embryos (Figures 1 and 5A). In contrast, only 20% ($N = 74$) of the *six cycB* embryos looked like controls. In all the other *six cycB* embryos at cycle 10, nuclei at the anterior and the anterior-medial regions lagged behind and did not reach the cortex (Figure 5B). We analyzed some of the suppressor lines for this cycle 10 phenotype. The frequency of normal cycle 10 embryos is 85% for *chic$^{8893}$/six cycB* embryos ($N = 20$), 55% for *chic$^{7886}$/six cycB* embryos ($N = 22$), 72% for *qua$^{WP165}$/six cycB* embryos ($N = 85$), 80% for *cycA$^{C8LR1}$/six cycB* embryos ($N = 94$), and 71% for *sced$^{1}$/six cycB* embryos ($N = 35$). In contrast, a slight but not significant improvement was observed in *dia$^{2}$/six cycB* embryos (37% normal, $N = 24$) and no suppression of cycle 10 phenotype was observed in *zip$^{1}$/six cycB* embryos (20% normal, $N = 20$) and *Cdc42$^{2}$/six cycB* embryos (17% normal, $N = 66$). These observations are consistent with the astral microtubule morphology and Cdk1-CycB defects described earlier (Table 4).

**Astral microtubule morphology is consistent with antagonizing effects between microtubules and microfilaments in the syncytial embryos:** The observations that loss of *chic*, *qua*, and *sced* normalized astral microtubule morphology of *six cycB* preblastoderm embryos indicate that weakening the microfilament network strengthens microtubules. If the two cytoskeletal networks antagonize each other, we should observe this behavior in wild-type embryos. During cycles 4–9 of wild-type embryos, we noted more organized and longer microfilaments between the nuclear domain and the extended cortical region (von Dassow and Schubiger 1994; Figure 6A). If microfilaments antagonize microtubules, this uneven distribution of microfilaments should affect microtubule morphology.

We focused our analyses on astral microtubule morphology at metaphase and anaphase between cycles 7 and 9. During these cycles, nuclei initiate cortical migration (Foe and Alberts 1983) and thus enter a denser microfilament network (Figure 6A). We observed that the morphology of metaphase spindles in wild-type embryos at cycle 8 depends on the orientation of the spindle. As shown in Figure 6, B and C, the two asters of a spindle are similar in size if the metaphase spindle lies deep in the center of the embryo. However, metaphase spindles that oriented perpendicular to the surface of the embryo have asymmetric asters with small asters facing the cortex and large asters toward the embryo center. The most interesting aster configuration occurs when the spindle is parallel to the surface. Here astral microtubules facing the cortex are shorter than the ones directed toward the yolk (Figure 6, B and C). Similar observations are made during anaphase (data not shown). These observations suggest an antagonizing relationship between astral microtubules and the microfilament network.

We treated wild-type embryos with cytD (see materials and methods for details). After 10 min of cytD treatment, cortical microfilaments were depleted (Figure 6D). This treatment led to longer asters extending toward the embryo cortex at metaphase (Figure 6, E and F) and anaphase (data not shown). In contrast, the microtubule and microfilament morphology in embryos treated with Ringer's solution is similar to those illustrated in Figure 6, A and B. These observations support the hypothesis that astral microtubule and microfilament networks interact antagonistically in preblastoderm embryos.

## DISCUSSION

Coordination between cell-cycle progression and cytoskeletal dynamics is necessary for the normal progression of mitosis. Our genetic screen for deficiencies and genes that, when reduced in dosage would dominantly

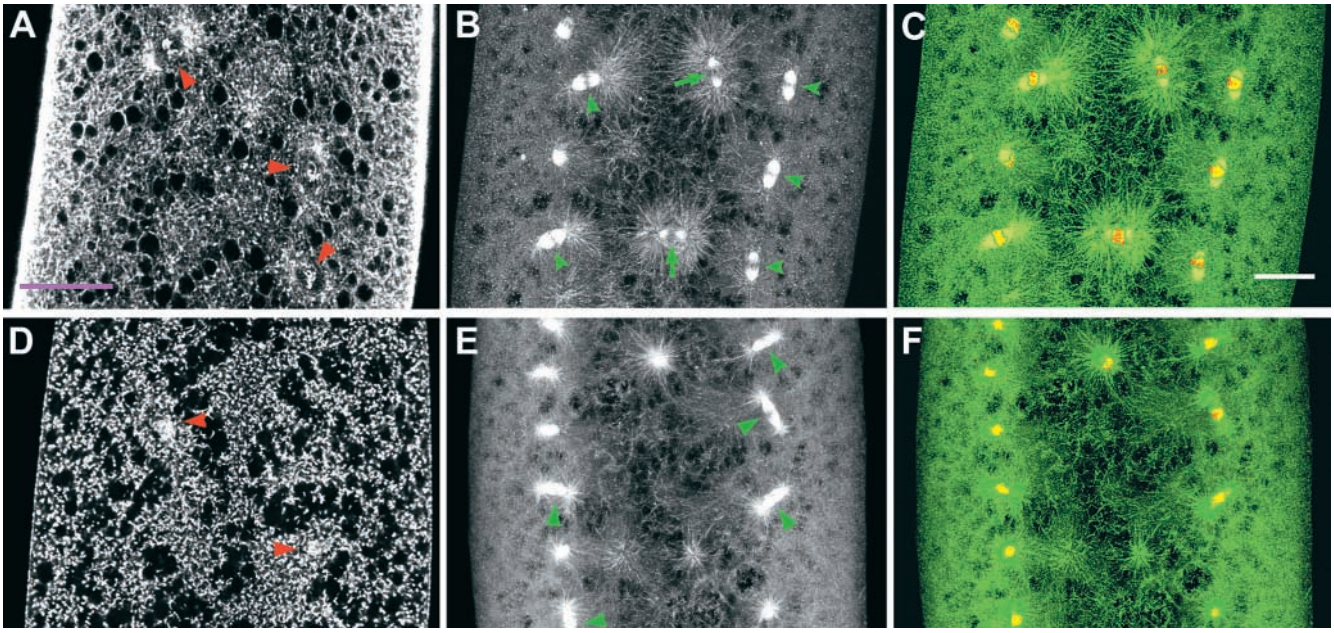


Figure 6.—Relationship between astral microtubule morphology and microfilament distribution at the extended cortex in cycle 8 wild-type embryos. (A–C) Control embryos. (D–F) cytD-treated embryos. (A) Denser microfilament network in the extended cortical region (purple line) in an embryo at metaphase. Red arrowheads indicate metaphase nuclei; this image is a single optical section. The embryo was stained with rhodamine-conjugated antihistone H1 antibody and BODIPY 558/568 phalloidin. (B) Asymmetric asters with shorter astral microtubules toward the cortex and longer astral microtubules toward the center (green arrowheads). Symmetric asters are shown in the deep interior region (green arrows). (C) The same image (microtubule in green) merged with anti-phospho-histone H3 staining (red) showing metaphase nuclei. B and C are projections of 9 optical sections with a 1-μm interval. Bar, 30 μm. (D) Cortical microfilaments are depleted after 10 min of cytD treatment. (E and F) Compared to B and C, asters are more symmetric in the extended cortical region in the cytD-treated wild-type embryos. E and F are projections of 12 sections with a 1-μm interval.

suppress the *six cycB* phenotypes, identified 10 suppressor genes, 7 of which are microfilament-related genes (Figure 7). Our analyses of astral microtubule morphology and Cdk1-CycB activity suggest that the interactions between Cdk1-CycB and two major components of the cytoskeletal network are important for normal cell-cycle progression and early embryonic development.

**Relation between Cdk1-CycB activities and microtubule dynamics:** We previously showed that higher Cdk1 activity reduces microtubule volume in the developing Drosophila embryo (Stiffler *et al.* 1999). Here we provided further evidence that metaphase astral microtubules were also sensitive to Cdk1 dosage. Furthermore, we found that loss of *cycA* had no effect on Cdk1-CycB activity, but astral microtubules were restored in *cycA/six cycB* embryos. These observations support the notion that both Cdk1-CycA and Cdk1-CycB can regulate microtubule dynamics (Verde *et al.* 1992).

Several observations indicated that CycB is degraded on microtubules. First, in many systems CycB is not degraded when microtubules are destroyed with microtubule-destabilizing drugs (Hunt *et al.* 1992; Maldonado-Codina and Glover 1992; Kubiak *et al.* 1993; Edgar *et al.* 1994). Second, CycB has to be degraded to progress through anaphase; it colocalizes with metaphase but not anaphase spindles in preblastoderm (Stiffler *et al.* 1999), syncytial blastoderm, and cellularized Drosophila embryos (Huang and Raff 1999). Finally, CycB and components of the anaphase-promoting complex/cyclosome, which is the CycB degradation machinery (Zachariae and Nasmyth 1999), coprecipitate with microtubules (Huang and Raff 1999). These

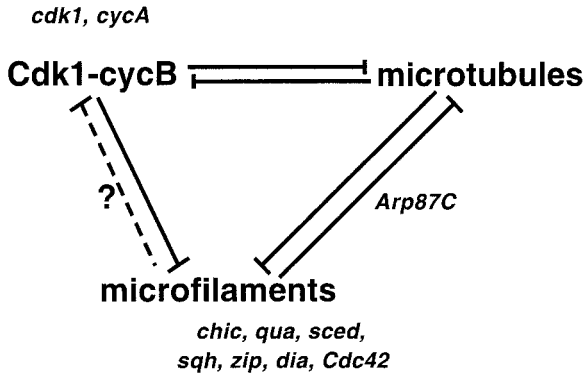


Figure 7.—Negative interactions among microtubules, microfilaments, and Cdk1-CycB. Microtubules and microfilaments interact antagonistically. Microfilament dynamics affect Cdk1-CycB activity during preblastoderm cycles; this effect likely occurs via microtubules (see discussion for details).

observations suggest that CycB degradation is sensitive to the state of the microtubules and that microtubules negatively affect Cdk1-CycB activities.

**Antagonistic effects between microtubules and microfilaments:** Work on yeast and Xenopus egg extracts identified protein complexes that mediate interactions between microtubules and microfilaments (Sider *et al.* 1999; Yin *et al.* 2000). One such complex is dynactin, which has been characterized in yeast and mammals (Schroer *et al.* 1996). In addition to organelle transport, the dynactin complex is involved in regulating spindle orientation and spindle rotation in both yeast and *Caenorhabditis elegans* (Muhua *et al.* 1994; Skop and White 1998). Both microtubules and microfilaments are required to regulate spindle orientation in yeast (Palmer *et al.* 1992) and spindle rotation in *C. elegans* (Hyman and White 1987). Dynactin also accumulates at microtubule distal ends in COS-7 cells (Vaughan *et al.* 1999). We have shown here that reducing Arp1 and Glued stabilizes microtubules in a *six cycB* background. These observations support the possibility that the dynactin complex normally has a destabilizing effect on astral microtubules and thus may contribute to the force necessary for spindle movement. This idea is also supported by the observation that loss of dynactin abolishes spindle rotation (Skop and White 1998), a process that requires the existence of cortical microfilament foci and shortening of astral microtubules (Hyman and White 1987; Waddle *et al.* 1994). We propose that astral microtubules and microfilaments antagonize each other and that the dynactin complex mediates this antagonizing effect. Perhaps the dynactin complex, which is anchored to the cortical microfilaments via its p62 subunit (Garces *et al.* 1999), controls microtubule dynamics. Whether dynein might participate in such an activity is not clear.

The hypothesis that the two major cytoskeletal networks antagonize each other is supported by our results with other suppressors, namely *chic*, *qua*, *sced*, *sqh* and *zip*. During oogenesis loss of *chic* (profilin) results in longer microtubules throughout the oocyte; a similar phenotype is observed with cytD treatment (Manseau *et al.* 1996). Profilin can promote microfilament growth at newly formed free barbed ends *in vitro* (Pantaloni and Carlier 1993; Kang *et al.* 1999). This agrees with the observation that overexpression of human profilin in CHO cells increases microfilament stability (Finkel *et al.* 1994). Therefore, reducing profilin may cause a less stable or less polymerized microfilament network, thereby permitting astral microtubules to grow longer. Similarly, the villin-like protein Qua has been shown to affect microfilament crosslinking or bundling during oogenesis (Mahajan-Miklos and Cooley 1994). The bundling of microfilaments could increase their stability, while reducing Qua could weaken microfilament stability. Also, the *sced* mutation severely disrupts microfilament organization (Stevenson *et al.* 2001). We show here that reducing Qua or Sced stabilizes microtubules. Reducing the myosin regulatory light chain (Sqh) or myosin heavy chain (Zip) may weaken microfilament network or microfilament contractility, thereby reducing the tension on microtubule networks, accounting for the more stable astral microtubules we observed.

Pharmacological studies further support this antagonistic interaction between microtubules and microfilaments. For example, in growth cones of cultured Aplysia neurons, microtubules are normally observed only in axons and the central domain of the growth cones while microfilaments are in the lamellar and peripheral region. Treatment of the growth cones with cytochalasin B removes microfilaments and results in rapid extension of microtubules into the lamellar and peripheral region (Forscher and Smith 1988). Consistent with this observation, treatment of unpolarized hippocampal neurons with either the cytD or the G-actin sequestering drug latrunculin B leads to neurons with multiple axon-like processes (Bradke and Dotti 1999). Similarly, treatment of cultured chick sensory neurons with nocodazole causes rapid axon retraction, while pretreatment with latrunculin or inhibition of myosin or dynein completely abolishes the retraction caused by nocodazole (Ahmad *et al.* 2000). Finally, our observations of asymmetric metaphase asters in the extended cortical region of wild-type embryos and more symmetric metaphase asters after cytD treatment at cycles 7–9 also support the antagonistic effect between the microtubules and microfilaments in the preblastoderm embryos (Figure 6).

The negative effect of microfilaments on Cdk1-CycB activity we observed may be either microtubule dependent or microtubule independent (Figure 7). For the following reasons, however, we favor the idea that the negative feedback from a weaker microfilament network on Cdk1-CycB activity occurs via microtubules. First, the identified suppressor proteins are members of complexes, such as Chic and components of the dynactin complex, which interact with microtubules. Second, we observed that lower levels of Sqh and Zip suppressed or partially suppressed the astral microtubule phenotype of *six cycB* embryos, but not Cdk1-CycB activity, indicating that the effect on the kinase activity is downstream of effects on microtubules. Third, drugs that directly destabilize microtubules indirectly prevent CycB degradation.

We have argued for the antagonizing effect between microtubules and microfilaments. However, the two networks have been shown to be cooperative in cases where microtubules are stable (Gavin 1999; Foe *et al.* 2000; Goode *et al.* 2000). During spermatogenesis in Drosophila, for example, microtubules in the central spindle and microfilaments in the contractile ring interact cooperatively: Disrupting either one of the structures weakens the assembly of the other (Giansanti *et al.* 1998).

**Suppression of the *six cycB* phenotypes occurs at different developmental stages:** We observed that loss of *cdk1*, *cycA*, *chic*, or *sced* in a *six cycB* background led to suppression of the *six cycB* phenotypes up to cycle 14:

Normalization of astral microtubules between cycles 5 and 7 brings the nuclei to the periphery at the correct time and nuclear density (cycle 10) and is followed by four normal blastoderm divisions (Table 4, class I). However, not all suppressors show this complete normalization. Loss of *Arp87C* rescues the Cdk1-CycB activity and astral microtubule morphology of the *six cycB* phenotype at cycles 5–7. At cycle 10 nuclear distribution is normal, but these embryos show no rescue at cycle 14 (Table 4, class II). In contrast, loss of *Cdc42* or *dia* rescues the *six cycB* phenotypes only after cycle 10 (Table 4, class III).

How do we account for the class II suppression pattern? Proteins such as Arp1 may associate with either a complex that has different targets or different complexes with different targets. In both scenarios, different targets could have different thresholds for their functions. Thus varying dosage of one component of the complex could lead to different phenotypes. For example, different levels of Lis1 (the β-subunit of platelet-activating factor acetylhydrolase isoform Ib) activity result in different phenotypes in mice: Slight reduction of the protein causes neuronal disorganization, further reduction causes more severe brain and cerebral defects, and complete deletion of Lis1 leads to early embryonic lethality (Hirotsune *et al.* 1998).

Class III suppressors rescue the *six cycB* phenotype after cycle 10. This type of suppression could be due to either a delay in translation of maternal mRNA after cycle 10 or localization of the proteins at the cortex that occurs only after cycle 10 and is necessary for the suppression. We observed that loss of one copy of *dia* suppressed only at cycle 14 but not before cycle 10. Since Dia is located at the cortex of the embryo during the syncytial blastoderm cycles and *dia* germ-line clone embryos develop normally up to cycle 10 (Afshar *et al.* 2000), Dia may assert its function only after cycle 10. Alternatively, the relative amount of a maternal gene product may decline as the embryo develops, and the embryo runs out of this product earlier with only one gene copy. This possibility could account for suppression only after cycle 10.

**Allelic difference in suppression of the *six cycB* phenotypes:** Suppression of a phenotype can be viewed as complementation between mutations of different genes (extragenic complementation). Testing multiple alleles of *chic*, *Cdc42*, and *sqh*, we observed suppression of the *six cycB* phenotypes with all but one hypomorphic allele. Interestingly, none of the null alleles suppressed. To account for this, we see two alternatives. Mutant proteins could compete with the normal protein and thus have an antimorphic effect. Alternatively, the mutant protein could have a deleterious effect and thus act as a neomorph. In both cases, null alleles would not have a phenotype. For examples, Hays *et al.* (1989) have shown that with extragenic complementation tests of the α-tubulin mutant allele $TubA84B^{nc33}$, the null allele of *TubA84B*, but not missense mutant allele $TubA84B^{nc33}$, complements with testis-specific β-tubulin gene *B2t* allele. Males with extra copies of $TubA84B^{nc33}$ are completely sterile, indicating the antimorphic effect of the $Tub\text{-}A84B^{nc33}$ allele (Hays *et al.* 1989). A neomorphic effect was suggested for *zipper* mutant alleles on the basis of extragenic complementation tests: The null allele $zip^{2}$ complements with *RhoGEF2* or *RhoA* alleles while the mutant allele $zip^{Ebr}$ does not, which could be due to a poisonous (neomorphic) effect of mutant Zip protein (Halsell *et al.* 2000). We favor the idea that suppression of the *six cycB* phenotypes is an antimorphic effect since four out of five *chic* hypomorphic alleles are suppressors of the *six cycB* phenotype, but none of them has a dominant phenotype. Also, we are not aware of any case where all tested hypomorphic alleles of a single gene are neomorphic.

The use of deficiencies in only a few cases produced the phenotype of a single-gene mutation in our screen. This could be due to the deletion of many genes within a single deficiency, where products of genes within deficiencies might have opposing effects on the cytoskeleton. Thus, it would be difficult to observe the genetic interaction of a deficiency that contains both an enhancer and a suppressor gene in our screen.

The observation that the hypomorphic alleles, in contrast to the null alleles, suppress the *six cycB* phenotype indicates a delicate balance among microtubules, microfilaments, and Cdk1-CycB. Disturbance of this balance produces a phenotype that is not lethal, suggesting that the system must be buffered to tolerate the observed imbalance. Further analyses on how these factors interact at a molecular level should provide insights on how the cell-cycle machinery interacts with the cytoskeletal network.

We are grateful to Chris Beach, Justin Crest, Craig Magie, Lisa Stiffler, Susanne Trautmann, and Tien Vuong for their help during the initial screen and Kim McClure for her help with the cytochalasin D injection experiment. We appreciate Amy Bejsovec, Lynn Cooley, Rick Fehon, Daniel Kiehart, Paul Lasko, Christian Lehner, Susan Parkhurst, Trudi Schüpbach, Bill Sullivan, and Steven Wasserman and the Bloomington and Umea stock centers for sharing mutant and deficiency stocks with us. We thank Will Whitfield and David Glover for the generous gift of CycB antiserum Rb271. We appreciate Victoria Foe, John Sisson, and George von Dassow for their advice on the phalloidin staining and Ray Huey for his help on the statistical analyses. We are grateful to Steve Jackson, Kim McClure, Margrit Schubiger, Glenn Yasuda, and two anonymous reviewers for very helpful comments on the manuscript. We also thank Drs. Buzz Baum, Bill Bement, Lynn Cooley, Bruce Edgar, Victoria Foe, Mike Goldberg, Roger Karess, Christian Lehner, Lynn Manseau, Kathryn Miller, Tim Mitchison, Pat O'Farrell, Jordan Raff, Greenfield Sluder, Trudi Schüpbach, Daniel St. Johnston, Bill Sullivan, and Bill Theurkauf for helpful discussions. This work was supported by National Science Foundation grant IBN 97-27944 to G.S. and National Institutes of Health grant GM35252 to L.S.B.G., an investigator of the Howard Hughes Medical Institute.

## LITERATURE CITED

Afshar, K., B. Stuart and S. A. Wasserman, 2000 Functional analysis of the Drosophila diaphanous FH protein in early embryonic development. Development **127:** 1887–1897.

Ahmad, F. J., J. Hughey, T. Wittmann, A. Hyman, M. Greaser *et al.*, 2000 Motor proteins regulate force interactions between

microtubules and microfilaments in the axon. Nat. Cell Biol. **2:** 276–280.

Baker, J., W. E. Theurkauf and G. Schubiger, 1993 Dynamic changes in microtubule configuration correlate with nuclear migration in the preblastoderm Drosophila embryo. J. Cell Biol. **122:** 113–121.

Bradke, F., and C. G. Dotti, 1999 The role of local actin instability in axon formation. Science **283:** 1931–1934.

Castrillon, D. H., and S. A. Wasserman, 1994 Diaphanous is required for cytokinesis in Drosophila and shares domains of similarity with the products of the limb deformity gene. Development **120:** 3367–3377.

Castrillon, D. H., P. Gonczy, S. Alexander, R. Rawson, C. G. Eberhart *et al.*, 1993 Toward a molecular genetic analysis of spermatogenesis in *Drosophila melanogaster*: characterization of male-sterile mutants generated by single *P*-element mutagenesis. Genetics **135:** 489–505.

Clegg, N. J., I. P. Whitehead, J. A. Williams, G. B. Spiegelman and T. A. Grigliatti, 1993 A developmental and molecular analysis of Cdc2 mutations in *Drosophila melanogaster*. Genome **36:** 676–685.

Cooley, L., E. Verheyen and K. Ayers, 1992 *chickadee* encodes a profilin required for intercellular cytoplasm transport during Drosophila oogenesis. Cell **69:** 173–184.

Edgar, B. A., F. Sprenger, R. J. Duronio, P. Leopold and P. H. O'Farrell, 1994 Distinct molecular mechanisms regulate cell cycle timing at successive stages of Drosophila embryogenesis. Genes Dev. **8:** 440–452.

Edwards, K. A., and D. P. Kiehart, 1996 Drosophila nonmuscle myosin II has multiple essential roles in imaginal disc and egg chamber morphogenesis. Development **122:** 1499–1511.

Evangelista, M., K. Blundell, M. S. Longtine, C. J. Chow, N. Adames *et al.*, 1997 Bni1p, a yeast formin linking Cdc42p and the actin cytoskeleton during polarized morphogenesis. Science **276:** 118–122.

Finkel, T., J. A. Theriot, K. R. Dise, G. F. Tomaselli and P. J. Goldschmidt-Clermont, 1994 Dynamic actin structures stabilized by profilin. Proc. Natl. Acad. Sci. USA **91:** 1510–1514.

FlyBase Consortium 1999 The FlyBase database of the *Drosophila* genome projects and community literature. Nucleic Acids Res. **27**: 85–88 (http://flybase.bio.indiana.edu/).

Foe, V. E., and B. M. Alberts, 1983 Studies of nuclear and cytoplasmic behavior during the five mitotic cycles that precede gastrulation in Drosophila embryogenesis. J. Cell Sci. **61:** 31–70.

Foe, V. E., C. M. Field and G. M. Odell, 2000 Microtubules and mitotic cycle phase modulate spatiotemporal distributions of F-actin and myosin II in Drosophila syncytial blastoderm embryos. Development **127:** 1767–1787.

Forscher, P., and S. J. Smith, 1988 Actions of cytochalasins on the organization of actin filaments and microtubules in a neuronal growth cone. J. Cell Biol. **107:** 1505–1516.

Fyrberg, C., L. Ryan, M. Kenton and E. Fyrberg, 1994 Genes encoding actin-related proteins of Drosophila melanogaster. J. Mol. Biol. **241:** 498–503.

Garces, J. A., I. B. Clark, D. I. Meyer and R. B. Vallee, 1999 Interaction of the p62 subunit of dynactin with Arp1 and the cortical actin cytoskeleton. Curr. Biol. **9:** 1497–1500.

Gavin, R. H., 1999 Synergy of cytoskeleton components. Bioscience **49:** 641–655.

Genova, J. L., S. Jong, J. T. Camp and R. G. Fehon, 2000 Functional analysis of Cdc42 in actin filament assembly, epithelial morphogenesis, and cell signaling during Drosophila development. Dev. Biol. **221:** 181–194.

Giansanti, M. G., S. Bonaccorsi, B. Williams, E. V. Williams, C. Santolamazza *et al.*, 1998 Cooperative interactions between the central spindle and the contractile ring during Drosophila cytokinesis. Genes Dev. **12:** 396–410.

Goldstein, L. S., and S. Gunawardena, 2000 Flying through the Drosophila cytoskeletal genome. J. Cell Biol. **150:** F63–F68.

Goode, B. L., D. G. Drubin and G. Barnes, 2000 Functional cooperation between the microtubule and actin cytoskeletons. Curr. Opin. Cell Biol. **12:** 63–71.

Haghnia, M., A. Bowman, M. McGrail and L. S. B. Goldstein, 2001 Study of two axonal transport mutants in Drosophila, ARP1 (Actin Related Protein) and redtape. A. Dros. Res. Conf. **42:** 204C.

Halsell, S. R., B. I. Chu and D. P. Kiehart, 2000 Genetic analysis demonstrates a direct link between Rho signaling and nonmuscle myosin function during Drosophila morphogenesis. Genetics **155:** 1253–1265.

Hartley, R. S., R. E. Rempel and J. L. Maller, 1996 In vivo regulation of the early embryonic cell cycle in Xenopus. Dev. Biol. **173:** 408–419.

Hays, T. S., R. Deuring, B. Robertson, M. Prout and M. T. Fuller, 1989 Interacting proteins identified by genetic interactions: a missense mutation in α-tubulin fails to complement alleles of the testis-specific β-tubulin gene of *Drosophila melanogaster*. Mol. Cell. Biol. **9:** 875–884.

Hirotsune, S., M. W. Fleck, M. J. Gambello, G. J. Bix, A. Chen *et al.*, 1998 Graded reduction of Pafah1b1 (Lis1) activity results in neuronal migration defects and early embryonic lethality. Nat. Genet. **19:** 333–339.

Huang, J. Y., and J. W. Raff, 1999 The disappearance of cyclin B at the end of mitosis is regulated spatially in Drosophila cells. EMBO J. **18:** 2184–2195.

Hunt, T., F. C. Luca and J. V. Ruderman, 1992 The requirements for protein synthesis and degradation, and the control of destruction of cyclins A and B in the meiotic and mitotic cell cycles of the clam embryo. J. Cell Biol. **116:** 707–724.

Hyman, A. A., and J. G. White, 1987 Determination of cell division axes in the early embryogenesis of *Caenorhabditis elegans*. J. Cell Biol. **105:** 2123–2135.

Jacobs, H. W., J. A. Knoblich and C. F. Lehner, 1998 Drosophila Cyclin B3 is required for female fertility and is dispensable for mitosis like Cyclin B. Genes Dev. **12:** 3741–3751.

Kang, F., D. L. Purich and F. S. Southwick, 1999 Profilin promotes barbed-end actin filament assembly without lowering the critical concentration. J. Biol. Chem. **274:** 36963–36972.

Karess, R. E., X. J. Chang, K. A. Edwards, S. J. Kulkarni, I. Aguilera *et al.*, 1991 The regulatory light chain of nonmuscle myosin is encoded by *spaghetti-squash*, a gene required for cytokinesis in Drosophila. Cell **65:** 1177–1189.

Kennison, J. A., and J. W. Tamkun, 1988 Dosage-dependent modifiers of Polycomb and Antennapedia mutations in Drosophila. Proc. Natl. Acad. Sci. USA **85:** 8136–8140.

Kim, S. H., C. Li and J. L. Maller, 1999 A maternal form of the phosphatase Cdc25A regulates early embryonic cell cycles in *Xenopus laevis*. Dev. Biol. **212:** 381–391.

Kubiak, J. Z., M. Weber, H. de Pennart, N. J. Winston and B. Maro, 1993 The metaphase II arrest in mouse oocytes is controlled through microtubule-dependent destruction of cyclin B in the presence of CSF. EMBO J. **12:** 3773–3778.

Lee, L. A., L. K. Elfring, G. Bosco and T. L. Orr-Weaver, 2001 A genetic screen for suppressors and enhancers of the Drosophila PAN GU cell cycle kinase identifies Cyclin B as a target. Genetics **158:** 1545–1556.

Li, W., E. Noll and N. Perrimon, 2000 Identification of autosomal regions involved in Drosophila Raf function. Genetics **156:** 763–774.

Limbourg, R., and M. Zalokar, 1973 Permeabilization of Drosophila eggs. Dev. Biol. **35:** 382–387.

Mahajan-Miklos, S., and L. Cooley, 1994 Intercellular cytoplasm transport during Drosophila oogenesis. Dev. Biol. **165:** 336–351.

Maldonado-Codina, G., and D. Glover, 1992 Cyclins A and B associate with chromatin and the polar regions of spindles, respectively, and do not undergo complete degradation at anaphase in syncytial Drosophila embryos. J. Cell Biol. **116:** 967–976.

Manseau, L., J. Calley and H. Phan, 1996 Profilin is required for posterior patterning of the Drosophila oocyte. Development **122:** 2109–2116.

Mitchison, T. J., and J. Sedat, 1983 Localization of antigenic determinants in whole Drosophila embryos. Dev. Biol. **99:** 261–264.

Morgan, D. O., 1995 Principles of CDK regulation. Nature **374:** 131–134.

Muhua, L., T. S. Karpova and J. A. Cooper, 1994 A yeast actin-related protein homologous to that in vertebrate dynactin complex is important for spindle orientation and nuclear migration. Cell **78:** 669–679.

Murray, A. W., and T. Hunt, 1993 *The Cell Cycle: An Introduction*. W. H. Freeman, New York.

Murray, A. W., and M. W. Kirschner, 1989 Cyclin synthesis drives the early embryonic cell cycle. Nature **339:** 275–280.

Newman, S. M., Jr., and G. Schubiger, 1980 A morphological and developmental study of Drosophila embryos ligated during nuclear multiplication. Dev. Biol. **79:** 128–138.

Nicholls, R. E., and W. M. Gelbart, 1998 Identification of chromosomal regions involved in *decapentaplegic* function in Drosophila. Genetics **149:** 203–215.

Nurse, P., 1990 Universal control mechanism regulating onset of M-phase. Nature **344:** 503–508.

Palmer, R. E., D. S. Sullivan, T. Huffaker and D. Koshland, 1992 Role of astral microtubules and actin in spindle orientation and migration in the budding yeast, *Saccharomyces cerevisiae*. J. Cell Biol. **119:** 583–593.

Pantaloni, D., and M. F. Carlier, 1993 How profilin promotes actin filament assembly in the presence of thymosin beta 4. Cell **75:** 1007–1014.

Price, D., S. Rabinovitch, P. H. O'Farrell and S. D. Campbell, 2000 Drosophila *wee1* has an essential role in the nuclear divisions of early embryogenesis. Genetics **155:** 159–166.

Schroer, T. A., J. B. Bingham and S. R. Gill, 1996 Actin-related protein 1 and cytoplasmic dynein-based motility—What's the connection? Trends Cell Biol. **6:** 212–215.

Schüpbach, T., and E. Wieschaus, 1991 Female sterile mutations on the second chromosome of Drosophila melanogaster. II. Mutations blocking oogenesis or altering egg morphology. Genetics **129:** 1119–1136.

Sibon, O. C., V. A. Stevenson and W. E. Theurkauf, 1997 DNA-replication checkpoint control at the Drosophila midblastula transition. Nature **388:** 93–97.

Sibon, O. C., A. Laurencon, R. Hawley and W. E. Theurkauf, 1999 The Drosophila ATM homologue Mei-41 has an essential checkpoint function at the midblastula transition. Curr. Biol. **9:** 302–312.

Sider, J. R., C. A. Mandato, K. L. Weber, A. J. Zandy, D. Beach *et al.*, 1999 Direct observation of microtubule-f-actin interaction in cell free lysates. J. Cell Sci. **112:** 1947–1956.

Sisson, J. C., C. Field, R. Ventura, A. Royou and W. Sullivan, 2000 Lava lamp, a novel peripheral Golgi protein, is required for *Drosophila melanogaster* cellularization. J. Cell Biol. **151:** 905–918.

Skop, A. R., and J. G. White, 1998 The dynactin complex is required for cleavage plane specification in early *Caenorhabditis elegans* embryos. Curr. Biol. **8:** 1110–1116.

Stern, B., G. Ried, N. J. Clegg, T. A. Grigliatti and C. F. Lehner, 1993 Genetic analysis of the Drosophila cdc2 homolog. Development **117:** 219–232.

Stevenson, V. A., J. Kramer, J. Kuhn and W. E. Theurkauf, 2001 Centrosomes and the Scrambled protein coordinate microtubule-independent actin reorganization. Nat. Cell Biol. **3:** 68–75.

Steward, R., and C. Nüsslein-Volhard, 1986 The genetics of the dorsal-Bicaudal-D region of *Drosophila melanogaster*. Genetics **113:** 665–678.

Stiffler, L. A., J. Y. Ji, S. Trautmann, C. Trusty and G. Schubiger, 1999 Cyclin A and B functions in the early Drosophila embryo. Development **126:** 5505–5513.

Su, T. T., F. Sprenger, P. J. DiGregorio, S. D. Campbell and P. H. O'Farrell, 1998 Exit from mitosis in Drosophila syncytial embryos requires proteolysis and cyclin degradation, and is associated with localized dephosphorylation. Genes Dev. **12:** 1495–1503.

Sullivan, W., P. Fogarty and W. Theurkauf, 1993 Mutations affecting the cytoskeletal organization of syncytial Drosophila embryos. Development **118:** 1245–1254.

Swaroop, A., M. L. Paco-Larson and A. Garen, 1985 Molecular genetics of a transposon-induced dominant mutation in the Drosophila locus *Glued*. Proc. Natl. Acad. Sci. USA **82:** 1751–1755.

Theurkauf, W. E., 1992 Behavior of structurally divergent alpha-tubulin isotypes during Drosophila embryogenesis: evidence for post-translational regulation of isotype abundance. Dev. Biol. **154:** 205–217.

Vaughan, K. T., S. H. Tynan, N. E. Faulkner, C. J. Echeverri and R. B. Vallee, 1999 Colocalization of cytoplasmic dynein with dynactin and CLIP-170 at microtubule distal ends. J. Cell Sci. **112:** 1437–1447.

Verde, F., J. C. Labbe, M. Doree and E. Karsenti, 1990 Regulation of microtubule dynamics by cdc2 protein kinase in cell-free extracts of Xenopus eggs. Nature **343:** 233–238.

Verde, F., M. Dogterom, E. Stelzer, E. Karsenti and S. Leibler, 1992 Control of microtubule dynamics and length by cyclin A- and cyclin B-dependent kinases in Xenopus egg extracts. J. Cell Biol. **118:** 1097–1108.

Verheyen, E., and L. Cooley, 1994 Profilin mutations disrupt multiple actin-dependent processes during Drosophila development. Development **120:** 717–728.

von Dassow, G., and G. Schubiger, 1994 How an actin network might cause fountain streaming and nuclear migration in the syncytial Drosophila embryo. J. Cell Biol. **127:** 1637–1653.

Waddle, J. A., J. A. Cooper and R. H. Waterston, 1994 Transient localized accumulation of actin in *Caenorhabditis elegans* blastomeres with oriented asymmetric divisions. Development **120:** 2317–2328.

Wasserman, S., 1998 FH proteins as cytoskeletal organizers. Trends Cell Biol. **8:** 111–115.

Yamashiro, S., H. Chern, Y. Yamakita and F. Matsumura, 2001 Mutant Caldesmon lacking cdc2 phosphorylation sites delays M-phase entry and inhibits cytokinesis. Mol. Biol. Cell **12:** 239–250.

Yin, H., D. Pruyne, T. C. Huffaker and A. Bretscher, 2000 Myosin V orientates the mitotic spindle in yeast. Nature **406:** 1013–1015.

Zachariae, W., and K. Nasmyth, 1999 Whose end is destruction: cell division and the anaphase-promoting complex. Genes Dev. **13:** 2039–2058.

Zalokar, M., and I. Erk, 1976 Division and migration of nuclei during early embryogenesis of *Drosophila melanogaster*. J. Microscopie Biol. Cell **25:** 97–106.

Zar, J. H., 1999 *Biostatistical Analysis*, Ed. 4. Prentice-Hall, Englewood Cliffs, NJ.

Communicating editor: T. Schüpbach